iScience

CellPress
OPEN ACCESS

Article

Non-canonical type 1 cannabinoid receptor signaling regulates night visual processing in the inner rat retina

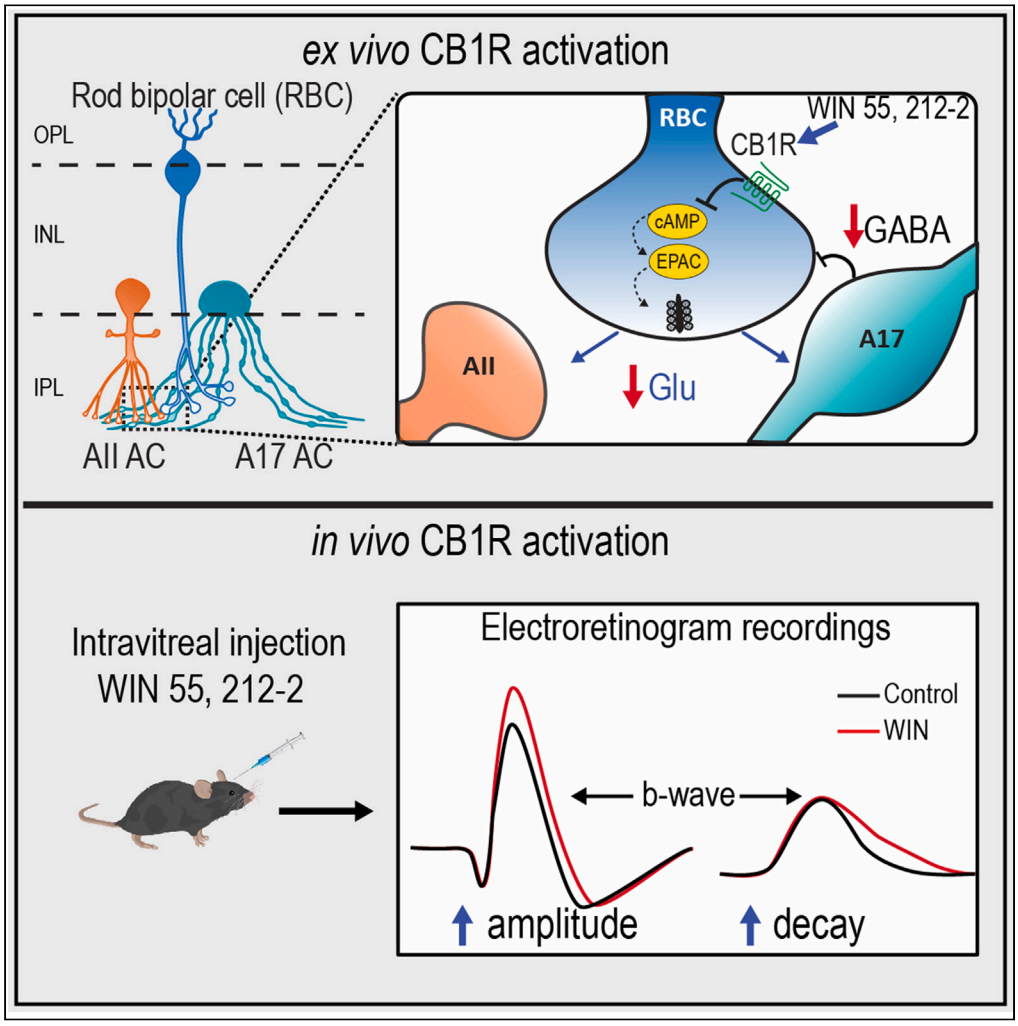

Sebastián F. Estay, Camila Morales-Moraga, Alex H. Vielma, Angelina Palacios-Muñoz, Chiayu Q. Chiu, Andrés E. Chávez

andres.chavez@uv.cl

Highlights

CB1 receptors (CB1Rs) are expressed in mammalian retinal rod bipolar cells (RBCs)

In RBC, the activation of CB1R decreases glutamate release via the cAMP-EPAC pathway

By reducing glutamate release, CB1R ablate reciprocal inhibitory signal onto RBC

CB1R also modulates rod-driven light responses *in vivo* to fine-tune night vision

Estay et al., iScience 27, 109920
June 21, 2024
https://doi.org/10.1016/j.isci.2024.109920

iScience

CellPress
OPEN ACCESS

Article

Non-canonical type 1 cannabinoid receptor signaling regulates night visual processing in the inner rat retina

Sebastián F. Estay,[1,2] Camila Morales-Moraga,[2] Alex H. Vielma,[2] Angelina Palacios-Muñoz,[2,3] Chiayu Q. Chiu,[2] and Andrés E. Chávez[2,4,*]

SUMMARY

Type 1 cannabinoid receptors (CB1Rs) are expressed in major retinal neurons within the rod-pathway suggesting a role in regulating night visual processing, but the underlying mechanisms remain poorly understood. Using acute rat retinal slices, we show that CB1R activation reduces glutamate release from rod bipolar cell (RBC) axon terminals onto AII and A17 amacrine cells through a pathway that requires exchange proteins directly activated by cAMP (EPAC1/2) signaling. Consequently, CB1R activation abrogates reciprocal GABAergic feedback inhibition from A17 amacrine cells. Moreover, the activation of CB1Rs *in vivo* enhances and prolongs the time course of the dim-light rod-driven visual responses, an effect that was eliminated when both $GABA_A$ and $GABA_C$ receptors were blocked. Altogether, our findings underscore a non-canonical mechanism by which cannabinoid signaling regulates RBC dyad synapses in the inner retina to regulate dim-light visual responses to fine-tune night vision.

INTRODUCTION

The type 1 cannabinoid receptor (CB1R), one of the most widely expressed G protein–coupled receptors in the brain,[1] is known to serve as a key regulator of synaptic function and neuronal activity[2,3] and thus impact cognitive and sensory processing.[4,5] In the mammalian retina, increasing evidence supports the expression of CB1Rs in both the inner and outer retina of several species, including rats and humans suggesting that they may play a significant role in retinal sensory processing.[6–15] For instance, anecdotal[16] and experimental evidence reported changes in night vision after cannabis consumption.[17–20] More recently, CB1R activation reportedly improves visual contrast sensitivity under low-light conditions in tadpoles.[21] However, a clear picture of the mechanisms by which CB1Rs regulate night visual processing has not yet emerged.

Rod photoreceptors mediate night vision by making glutamatergic synapses onto ON-type rod bipolar cells (RBCs), which in turn establish glutamatergic ribbon synapses onto two postsynaptic amacrine cells (ACs): the glycinergic AII and the GABAergic A17 AC.[22,23] While AII ACs transfer rod signals to the cone pathway and divide them into ON and OFF components,[24] A17 ACs provide reciprocal GABAergic feedback inhibition onto the RBC axon terminal[23,25–28] that contributes to the termination of rod signals, especially those elicited in dim-light conditions.[29] RBC terminals also receive lateral non-reciprocal inhibitory inputs from distinct types of ACs,[30,31] which modulate RBC activity and visual responses depending on the degree of light adaptation.[32–38] Notably, CB1R expression has been reported within the synaptic terminals of both rod photoreceptors and RBCs,[7,10,39] being well-positioned to fine-tune parallel feedforward excitatory transmission in both the outer and inner retina. However, whether and how CB1Rs regulate synaptic function at RBC dyad synapses and their impact on regulating night visual processing remains unknown.

To address these questions, we investigated the role of CB1Rs in regulating RBC dyad synapses in acute rat retinal slices and rod-driven responses *in vivo*. Our results indicate that CB1R activation reduces glutamate release from RBC ribbon synapses onto postsynaptic AII and A17 amacrine cells, requiring a non-canonical signaling pathway that involves G-protein α, cAMP, and EPAC1/2 function presynaptically. Moreover, reciprocal GABAergic feedback inhibition onto RBC axon terminals is also reduced. In addition, *in vivo* electroretinogram (ERG) recordings under scotopic conditions reveal a change in the b-wave of dim-light responses following CB1R activation. Taken together, our findings suggest that the recruitment of CB1Rs in this evolutionarily conserved retinal microcircuit may improve night vision by disinhibiting reciprocal feedback onto RBC axon terminals and increasing signal gain.

[1]Programa de Doctorado en Ciencias, Mención Neurociencia, Valparaíso 2340000, Chile
[2]Centro Interdisciplinario de Neurociencia de Valparaíso (CINV), Instituto de Neurociencias, Facultad de Ciencias, Universidad de Valparaíso, Valparaíso 2340000, Chile
[3]Present address: Centro de Investigación en Ciencias Odontológicas y Médicas (CICOM), Facultad de Odontología, Universidad de Valparaíso, 2340000, Chile
[4]Lead contact
*Correspondence: andres.chavez@uv.cl
https://doi.org/10.1016/j.isci.2024.109920

RESULTS

Type 1 cannabinoid receptor activation reduces glutamate release from rod bipolar cell axon terminals

CB1Rs may regulate excitatory activity in the inner retina. To test this possibility, we recorded spontaneous excitatory postsynaptic currents (sEPSCs) from morphologically identified A17 and AII ACs (V_{hold} = −60 mV) in acute rat retinal slices (see STAR Methods and Figures 1A and 1B). Pharmacological activation of CB1Rs with the agonist WIN 55,212-2 (WIN, 1 μM) for 10 min significantly reduced the frequency, but not the amplitude of sEPSCs recorded from A17 ACs (Figure 1A; also see Table S1 for all statistical numbers), consistent with a presynaptic mechanism of action of CB1Rs at the RBC axon terminal. Likewise, the frequency of sEPSCs recorded from AII ACs decreased following CB1R activation (Figure 1B), but a small, albeit significant, reduction of the sEPSC amplitude was also observed. Similarly, a slight but significant change in the amplitude of sEPSC was observed over time in AII ACs from control naive slices (Figure S1), suggesting a CB1R-independent mechanism.

To further confirm the involvement of CB1Rs in the downregulation of glutamate release from RBC terminals, retinal slices were preincubated with the CB1R inverse agonist, AM251 (4 μM for 10 min) and then continuously superfused during sEPSC recording. Under these experimental conditions, the CB1R-mediated effect on the frequency of sEPSC in AII ACs was abolished (Figure 1C). While WIN could also acts on CB2Rs,[40] we found that in the presence of the CB2R inverse agonist, AM630 (3 μM for 10 min), the WIN effect over sEPSC frequency remained intact (Figure 1D), indicating that CB1, but not CB2 receptors modulate glutamate release at RBC dyad synapses. Interestingly, the small reduction in sEPSC amplitude observed after the bath application of WIN (Figure 1B) was eliminated in AM251 and persisted in AM630, suggesting that CB1R may also be expressed, although to a very low extent, in AII ACs.[15]

Next, we evaluated whether the bath application of WIN could also reduce evoked EPSCs by performing paired recordings between synaptically connected RBCs and AII ACs. Depolarizing the presynaptic RBC (from −60 to −10 mV, 100 ms) elicited an EPSC in the postsynaptic AII AC, which was strongly reduced by CB1R activation (Figure 2A). Furthermore, depolarization also elicited a sustained inward Ca^{2+} current (I_{Ca}^{2+}) in the RBC, upon which a fast and transient, reciprocal feedback inhibitory postsynaptic current (vIPSC) was superimposed (Figure 2A). As reciprocal feedback is driven by RBC glutamate release onto A17 ACs, it serves as an indirect measure of glutamate release and would be expected to decrease concomitantly with reduced RBC exocytosis in the presence of a CB1R agonist (Figure 2A). Consistent with this idea, recordings of individual RBCs also showed that WIN reduces reciprocal vIPSCs (Figure 2B). Surprisingly, WIN did not affect the amplitude of sustained I_{Ca}^{2+} (Figures 2B and 2C). Together, these findings suggest that CB1R activation reduces feedforward and feedback signaling independent of the modulation of I_{Ca}^{2+} mediated by voltage-gated Ca^{2+} channels (VGCCs).

Type 1 cannabinoid receptors-mediated effects at rod bipolar cell terminals are independent of the inhibition of Ca^{2+} channels

To find the downstream signaling underlying the CB1R-mediated effects at the RBC dyad synapse, we next measured Ca^{2+} currents elicited at different voltage steps (from −90 to +30 mV, 20 mV steps; Figures 3A and 3B) or generated by a voltage ramp from −60 to +40 mV (Figure 3C). Bath application of WIN reduced superimposed reciprocal vIPSCs (Figure 3A) but did not affect the amplitude of the Ca^{2+} currents elicited by either voltage steps or voltage ramps (Figures 3A and 3C). To further corroborate these findings, we used two-photon laser scanning microscopy (2PLSM) to image Ca^{2+} transients (ΔCa^{2+}) at individual RBC axon terminals in the inner retina (Figure 3D). Consistent with the lack of Ca^{2+} current change, bath application of WIN did not suppress ΔCa^{2+} evoked by RBC depolarization (Figure 3E). In contrast, in control experiments performed in retinal ganglion cells (RGCs), where CB1Rs are known to inhibit Ca^{2+} signaling,[41] WIN significantly reduces ΔCa^{2+} evoked by RGC depolarization (Figure S2). These findings strongly support the idea that CB1R activation downregulates glutamate release at RBC terminals through a pathway that does not involve the inhibition of VGCCs.

Type 1 cannabinoid receptor-mediated effects require cAMP but not PKA signaling

Typically, CB1R-mediated inhibition of synaptic function involves the downregulation of presynaptic VGCCs via the βγ pathway or by inhibiting adenylyl cyclase via the $\alpha_{i/o}$ pathway.[2] If the modulation of VGCCs is not required for CB1R-mediated effects at RBC terminals, as suggested by the previous results, then blocking the G-protein βγ pathway should not occlude the WIN-mediated depression of glutamate release at the RBC-AII synapse. Accordingly, blockade of the G-protein βγ pathway with the specific antagonist gallein (GAL, 75 μM, 10 min) had no effect on the WIN-mediated depression of the sEPSC frequency and amplitude recorded from AII ACs (Figure 4A). In contrast, blocking the $\alpha_{i/o}$ pathway with the inhibitor NF-023 (NF, 10 μM, 10 min) occluded WIN-mediated effects (Figure 4B). Although NF alone substantially changed the frequency of sEPSCs, it could additionally be explained by its ability to modulate P2X purinergic receptors.[42] However, pre-treatment with the selective P2X receptor antagonist PPADS (10 μM, 10 min) did not block the effect of NF on sEPSCs (Figure S3), indicating that the CB1R-mediated depression of glutamate release from RBC terminals requires $\alpha_{i/o}$, but not βγ pathway.

Consequently, we then examined the involvement of cAMP/PKA dependent pathways by bath applying forskolin (FSK, 10 and 50 μM, 10 min), an activator of the adenylyl cyclase (Figure 4C) or the common PKA inhibitor, H89 (10 μM; Figure 4D). While FSK prevented the WIN-mediated depression of the sEPSC frequency (Figure 4C), H89 did not occlude the reduction induced by WIN (Figure 4D), further suggesting that cAMP, but not PKA signaling, is necessary for CB1R-mediated effects.

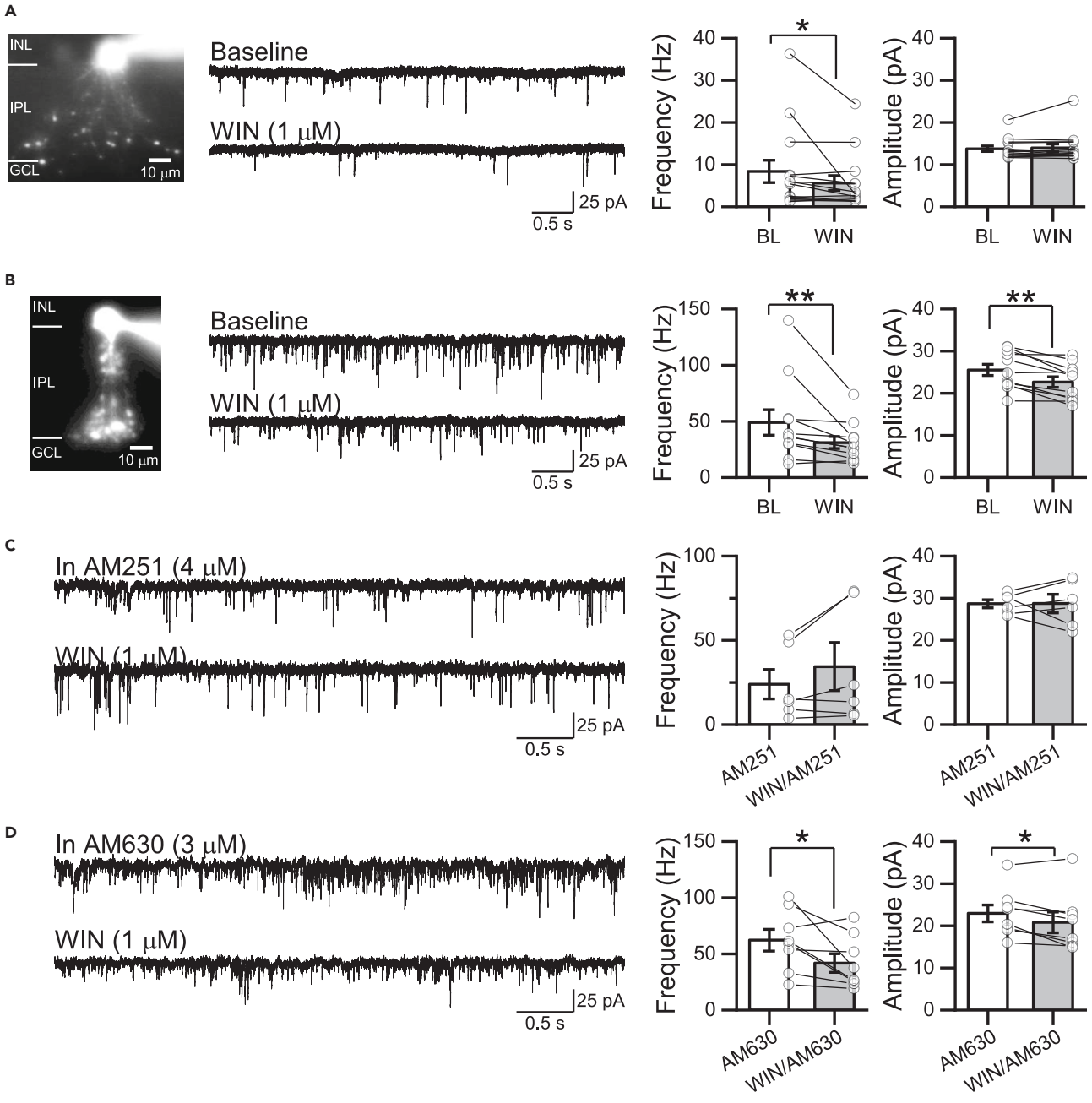

Figure 1. CB1 receptor activation reduces spontaneous excitatory inputs onto A17 and AII amacrine cells

(A) Representative image of A17 amacrine cell (AC) filled with Alexa Fluor 488 (*left*), representative traces of sEPSCs (V_{Hold} = −60 mV) during baseline (BL) and after the bath application of WIN (1 μM, *middle*), and summary graphs (*right*) showing that WIN decreased the frequency but not the amplitude of sEPSCs recorded in A17 ACs (n = 14 cells/11 animals).

(B) Representative image (*left*), representative traces (*middle*), and summary graphs showing that WIN also decreased the frequency of sEPSCs recorded in AII ACs (n = 11 cells/8 animals). Note that a small, reduction in the amplitude was also observed.

(C) Representative traces (*left*) and summary graphs (*right*) showing that WIN-mediated effects on sEPSC frequency and amplitude in AII ACs were blocked by pretreatment with the CB1R inverse agonist AM251 (4 μM, n = 6 cells/4 animals).

(D) Pretreatment with the CB2R inverse agonist AM630 (3 μM, n = 8 cells/5 animals) did not prevent the WIN-mediated effects on sEPSC frequency and amplitude in AII ACs. Data are presented as mean ± S.E.M and open circles represent a single cell. *p < 0.05, **p < 0.01. Comparisons were made using paired t-tests or Wilcoxon signed-rank tests. For statistics, see Table S1.

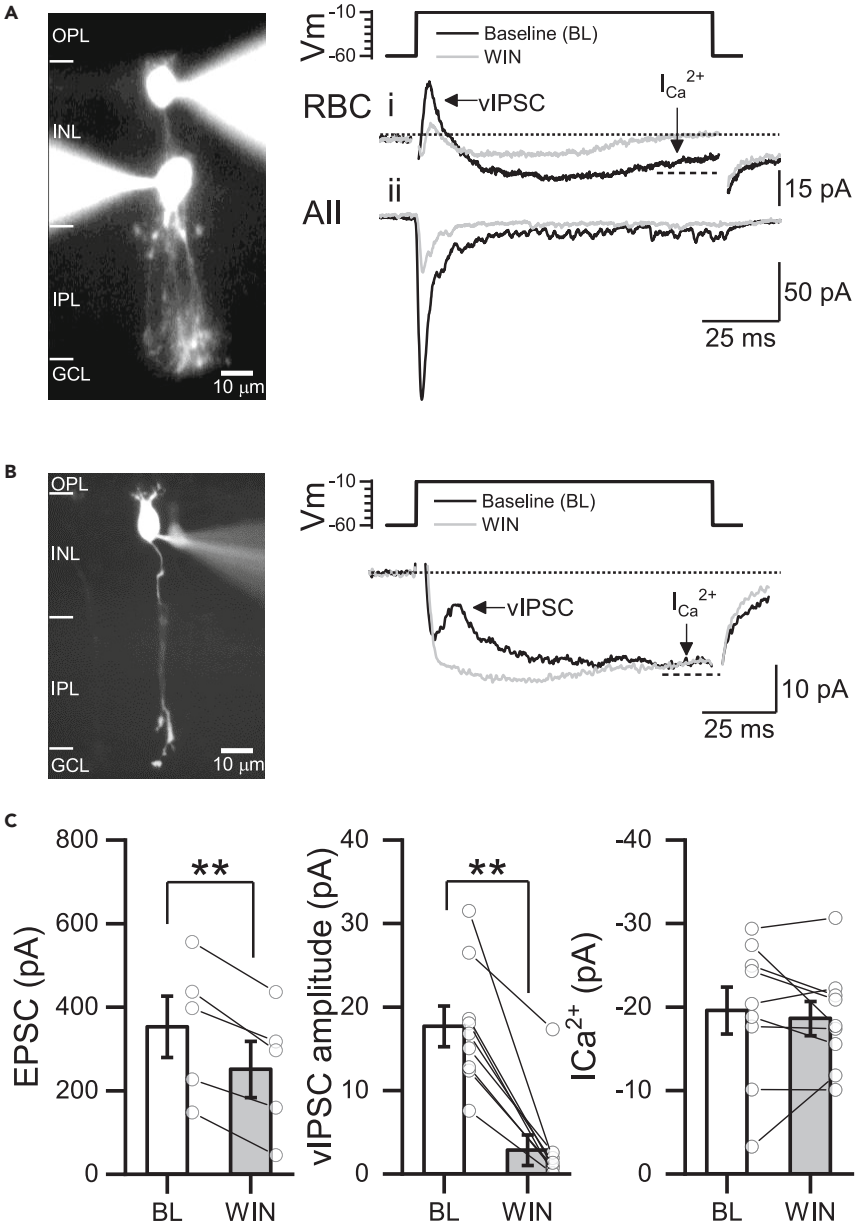

Figure 2. CB1R activation reduces feedforward excitation and reciprocal feedback inhibition at the RBC dyad synapse

(A) Paired whole-cell voltage-clamp recording of presynaptic rod bipolar cell (RBC) and postsynaptic AII AC filled with Alexa Fluor 488 (*left*). Representative traces showing the reciprocal voltage step evoked inhibitory postsynaptic current (vIPSC) recorded in the presynaptic RBC (i) and the EPSC recorded in the postsynaptic AII amacrine cell (ii) before (black trace) and after the bath application of WIN for 10 min (1 µM, gray trace, *right*). Currents were evoked by the depolarization of the presynaptic RBC (50 mV, 100 ms, from −60 to −10 mV).

(B) RBC filled with Alexa Fluor 488 (*left*) and representative vIPSC before (black trace) and after (gray trace) the bath application of WIN. Dotted line indicates where the inward Ca^{2+} current (I_{Ca}^{2+}) was measured at the end of the 100 ms step pulse.

(C) Summary graphs showing the effects of CB1R activation on the mean amplitude of the evoked EPSC (n = 5 cells, 5 animals, *left*), vIPSC amplitude (*middle*), and in the I_{Ca}^{2+} (*right*) before (BL) and after the bath application of WIN (n = 9 cells, 5 animals). I_{Ca}^{2+} was measured as the difference in the baseline (dotted line) and the last 20 ms of the inward current (dashed line). Recordings were performed in the presence of strychnine (3 µM) to block glycinergic inhibition and TTX (0.5 µM) to block lateral inhibition. Data are presented as mean ± S.E.M and open circles represent a single cell. $^{**}p < 0.01$. Comparisons were made using paired t-tests or Wilcoxon signed-rank tests. For statistics, see Table S1.

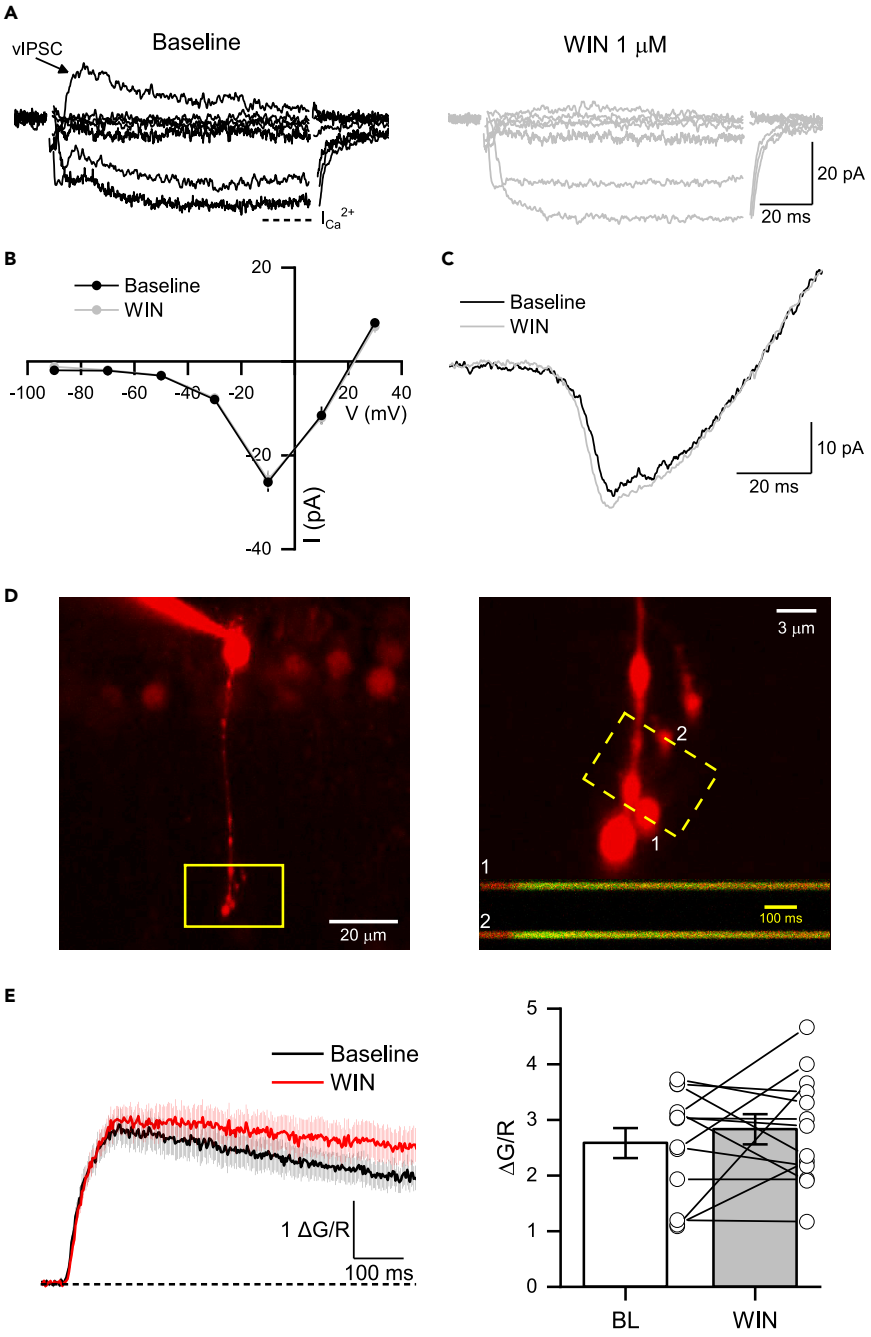

Figure 3. CB1R-mediated reduction of glutamate release is independent of the inhibition of voltage-gated Ca^{2+} channels in RBC terminals

(A) Voltage-clamp recordings elicited by depolarizing steps (from −90 to +30 mV, 20 mV steps) during baseline (BL, *left*) and after the bath application of WIN (1 μM, *right*). Note that the activation of CB1R eliminated reciprocal vIPSC (black arrow) elicited at different voltage steps without affecting the amplitude of the sustained inward Ca^{2+} currents (I_{Ca}^{2+}). Dotted line indicates where the I_{Ca}^{2+} was measured at the end of the 100 ms step pulse.

(B) Current-Voltage (I-V) curve showing that WIN had no effect on the amplitude of Ca^{2+} currents elicited by depolarizing voltage steps (n = 7 cells/5 animals).

(C) Representative voltage ramp depolarization from −90 to 30 mV before (black trace) and after (gray trace) the bath application of WIN.

(D) 2PLSM image of an RBC filled with Alexa Fluor 594 (*left*). Magnification shows RBC terminals line scanned (1 and 2) during a step-pulse depolarization (from −60 to −10 mV, 100 ms, *right*). Inset: Calcium transients (ΔCa^{2+}) scanned on terminals 1 and 2 during the depolarization step.

Figure 3. *Continued*

(E) Mean ΔCa^{2+} evoked by step-pulse depolarization before (black) and after WIN (red) bath application (*left*). Summary graphs showing that WIN had no effect on ΔCa^{2+} amplitude (n = 13 terminals/5 cells/5 animals). Data are presented as mean ± S.E.M and open circles represent a single terminal. Comparisons were made using paired t-tests. For statistics, see Table S1.

EPAC1/2 pathways are involved in the type 1 cannabinoid receptor-mediated effects at rod bipolar cell terminals

Although the cAMP-mediated modulation of neurotransmitter release has been attributed to the activation of PKA,[43–46] some evidence indicates that EPAC, an exchange protein directly activated by cAMP,[47,48] can mediate the PKA-independent regulation of transmitter release at central and sensory synapses.[49–54] More importantly, in the cerebellum, CB1Rs reportedly downregulate synaptic function in an EPAC-dependent manner.[55,56] To test this possibility at RBC dyad synapses, we used CE3F4 (50 μM, 10 min, Figure 5A), a specific inhibitor of EPAC1[57,58] and ESI-05 (10 μM, 10 min, Figure 5B), a selective EPAC2 antagonist.[59] While EPAC1 or EPAC2 inhibitors alone had no effect on sEPSC frequency and amplitude recorded from AII ACs, both antagonists were able to occlude WIN-mediated suppression of sEPSC frequency (Figures 5A and 5B), strongly suggesting that EPAC1/2 are involved in the CB1R-dependent regulation of glutamate release at RBC terminals.

Type 1 cannabinoid receptor activation increases the amplitude and shape of rod-driven light responses *in vivo*

Previous evidence indicates that the reciprocal GABAergic feedback inhibition onto RBC axon terminals plays an essential role in shaping the temporal characteristics of the dim light-evoked responses.[29] As the activation of CB1R reduces reciprocal vIPSCs in RBCs (Figure 2), the next logical step was to evaluate whether CB1R activation alters dim-light responses by performing *in vivo* ERG recordings before and after intravitreal injections of WIN (1 μM). Under dark adaptation conditions, the activation of CB1Rs led to a significant increase in the amplitude of ERG b-waves. This effect was independent of light intensity (Figure 6A) and reached a steady state around 15 min that persisted for up to 45 min post WIN injection (Figure S4A). Importantly, the increase in the ERG b-wave was CB1R-dependent as the co-administration of WIN with the CB1R inverse agonist AM251 (4 μM) eliminated the effect on the ERG b-waves amplitude (Figure 6B), and the vehicle (DMSO) infused alone, did not produce any effect (Figure S4B). In addition, the administration of WIN increased ERG a-wave but only at high light intensities (Figure 6A), an effect that was not eliminated by AM251 (Figure 6B), thus suggesting that WIN likely modulates other receptor types, besides CB1Rs, at the photoreceptor level to impact in the amplitude of the ERG a-wave at high-light stimulus intensity.[60–62]

To assess the temporal properties of the ERG b-wave, we measured the time to peak, the half-width of decay ($T_{½D}$), and the width (Figure 7). With dim-light stimulation, CB1R activation made ERG b-wave more sustained, significantly prolonging its decay and width (Figure 7A). This effect was not observed with bright-light stimulation (Figure S6A) and was not due to changes in the kinetics of ERG a-wave (Figure S6B), indicating that CB1Rs play a role in regulating the temporal properties of ERG b-wave under dim-light.

Because the amplitude and temporal characteristics of bipolar cell responses to light stimuli are shaped by GABAergic synaptic inhibition from ACs in the inner retina,[29,35,38,63,64] and CB1R activation decreases GABAergic reciprocal feedback (Figure 2), next we tested the efficacy of CB1Rs in regulating ERG b-wave in the presence of a mixture of the $GABA_A$ and $GABA_C$ receptor antagonists, SR95531 (5 μM) and TPMPA (10 μM). With GABA receptors blocked, the activation of CB1Rs no longer increased the amplitude (Figure 7B) nor prolonged the decay of the ERG b-wave (Figure 7C), supporting our hypothesis that CB1R activation regulates dim-light responses by modulating GABAergic synaptic transmission at RBC axon terminals within the rod pathway.

DISCUSSION

Here, using a combination of *ex vivo* single and cell-paired recordings with *in vivo* electrophysiological measurements, we uncover a mechanism by which CB1Rs modulate RBC dyad synapses in the inner retina to regulate the gain and temporal properties of dim-light visual responses. These findings may provide a mechanistic understanding of how cannabis consumption improves night vision. Moreover, our results indicate that CB1R activation reduces glutamatergic feedforward signaling from RBC onto AII and A17 ACs in a non-canonical way that does not involve calcium or PKA signaling. By downregulating glutamate release from RBC, CB1Rs reduce reciprocal inhibitory synapses onto RBC, therefore contributing to the regulation of visual processing of the dim-light response *in vivo*. Accordingly, we provide evidence that the activation of CB1R modifies the gain and the temporal properties of scotopic visual responses *in vivo*, an effect that is dependent on inhibitory transmission onto RBC. Altogether, our findings support a functional role for CB1Rs in regulating synaptic function to ultimately fine-tune visual processing in the inner mammalian retina.

Non-canonical type 1 cannabinoid receptor signaling regulates rod bipolar cell ribbon synapse

Although previous studies have shown that CB1Rs are expressed in different types of retinal bipolar cells, including rat RBCs,[6,7,13,15,65] and salamander bipolar cells,[10] our study has now demonstrated that the activation of CB1R regulates RBC synaptic function in the inner retina by reducing the frequency, but not the amplitude, of sEPSCs recorded in both postsynaptic elements, the AII and A17 ACs (Figure 1). Although it has been recently debated,[66,67] evidence also suggests that CB2Rs might be also expressed in RBC.[60,68,69] However, our data demonstrated that blocking CB1Rs but not CB2Rs eliminated the WIN-mediated depression of sEPSCs (Figure 1), indicating that in rat RBC terminals, CB1R rather than CB2Rs play an important role in regulating synaptic function. Consistent with this idea, the activation of CB1Rs also reduces evoked EPSCs in AII ACs and reciprocal vIPSCs elicited by RBCs depolarization (Figure 2). Interestingly, we also observed

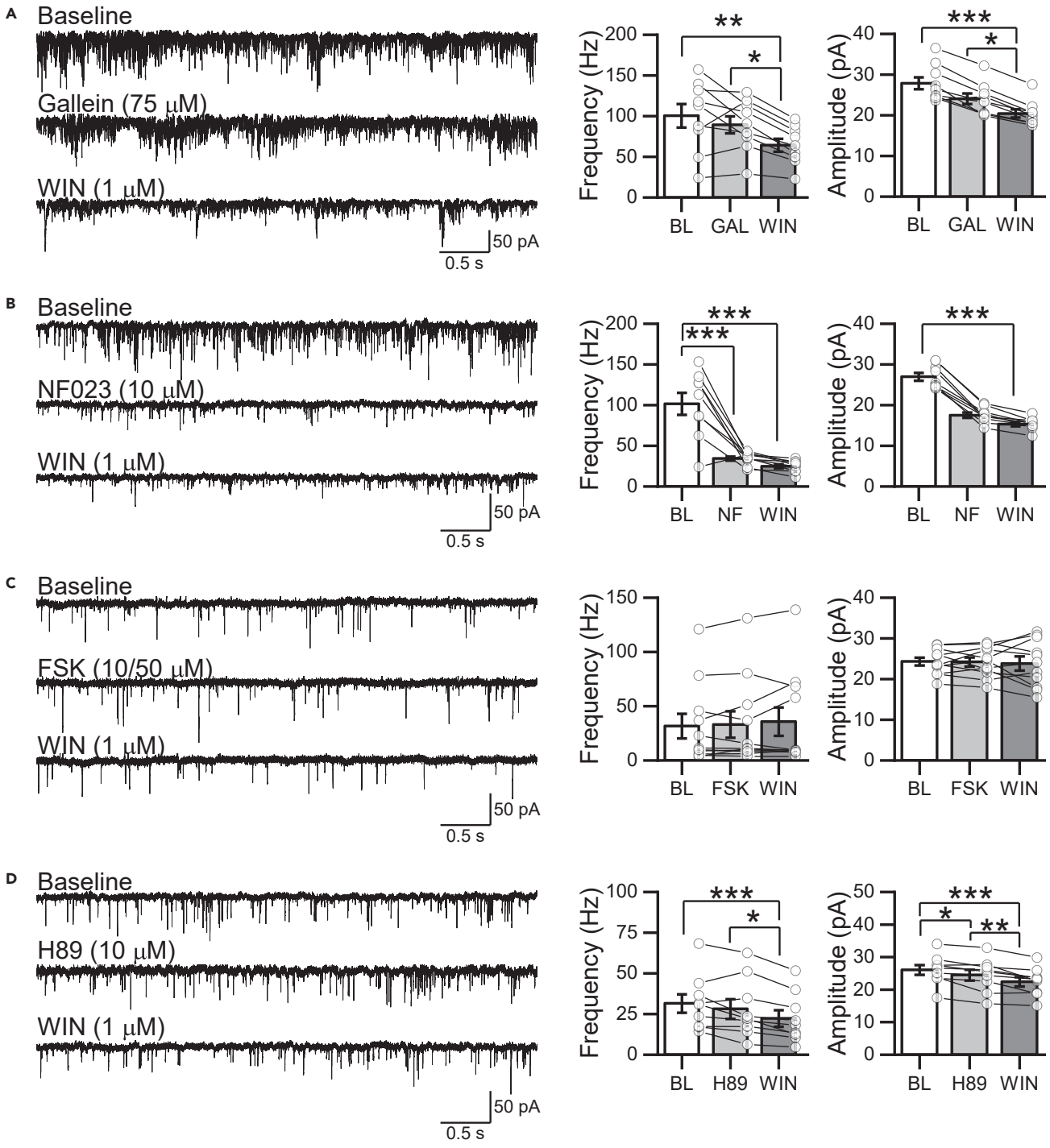

Figure 4. CB1R-mediated effects at RBC terminals involve G-protein αi/o in a cAMP-dependent, but PKA-independent manner

(A) Representative traces (*left*) and summary graphs (*right*) showing that the G-protein βγ inhibitor Gallein (75 μM) had no effect on WIN-mediated decrease of sEPSC frequency and amplitude in AII ACs (n = 9 cells/4 animals).

(B) Blocking G-protein αi/o with the inhibitor NF-023 (10 μM) strongly decreased the sEPSC frequency and occluded the WIN-mediated decrease of sEPSC frequency and amplitude in AII ACs (n = 9 cells/4 animals).

(C) Bath application of the adenylyl cyclase activator forskolin (FSK, data pooled for 10 and 50 μM) had no effect on the sEPSC frequency or amplitude but eliminated the WIN-mediated decrease of sEPSC frequency and amplitude in AII ACs (n = 11 cells/7 animals).

Figure 4. *Continued*

(D) Bath application of PKA inhibitor H89 (10 μM) decreased the sEPSC amplitude but did not prevent the WIN-mediated decrease of sEPSC frequency and amplitude in AII ACs (n = 9 cells/6 animals). Data are presented as mean ± S.E.M and open circles represent a single cell. *p < 0.05, **p < 0.01, ***p < 0.001. Multiple comparisons were made using one-way ANOVA-RM, followed by a post-hoc Tukey test, or using Friedman ANOVA followed by a post-hoc WMNT test. For statistics, see Table S1.

a small but significant effect in the amplitude of the sEPSC in AII ACs when CB1Rs were activated (Figure 1). This effect, which was not observed in the amplitude of sEPSCs recorded from A17 ACs and that was eliminated by blocking CB1Rs (Figure 1), opens the possibility that CB1Rs might be also present in AII ACs,[15] although to a much lower level than in RBC terminals. Further research is necessary to fully understand the conditions under which CB1Rs modulate AII AC function and, ultimately, how this modulation affects visual processing in the inner retina.

Multiple CB1R signaling pathways have been described to modulate synaptic function at central synapses, including the inhibition of presynaptic VGCCs via βγ signaling and inhibition of adenylyl cyclase and suppression of PKA activity likely mediated by $\alpha_{i/o}$ signaling.[2,70–75] Supporting this evidence, the activation of CB1Rs in retinal neurons has been shown to suppress Ca^{2+} influx in salamander bipolar cells[10] and ganglion cells.[13,41] However, our observations indicate that the activation of CB1R had no effect on the amplitude and/or dynamic of Ca^{2+} signaling in RBC terminals (Figures 2 and 3) and blocking βγ pathway did not prevent the reduction in sEPSC frequency induced by CB1R activation (Figure 4), suggesting that the adenylyl cyclase and suppression of PKA activity likely promoted the CB1R-mediated effect at the axon terminal of RBC. Accordingly, blocking $\alpha_{i/o}$ signaling or activating adenylyl cyclase abolished the CB1R-mediated reduction of the glutamate release (Figure 4). However, the blockade of PKA activity did not modify the glutamate release, indicating that CB1R-mediated effects in RBCs are PKA-independent. While PKA remains the classic substrate for cAMP, recent evidence has shown that EPAC, a cAMP-activated exchange protein,[47,76–78] acts as a downstream target of CB1Rs, dampening neurotransmitter release in cerebellar neurons.[55,56] Notably, both EPAC1 and EPAC2 are expressed in RBCs of the rat retina[79] and found in proximity to components of the vesicular release machinery at the synaptic ribbons.[80] In addition to the reported EPAC2-dependent enhancement of glycine release from AII AC onto OFF bipolar cells,[54] we now demonstrate that EPAC1 and/or EPAC2 independently block the CB1R-mediated reduction of glutamate release

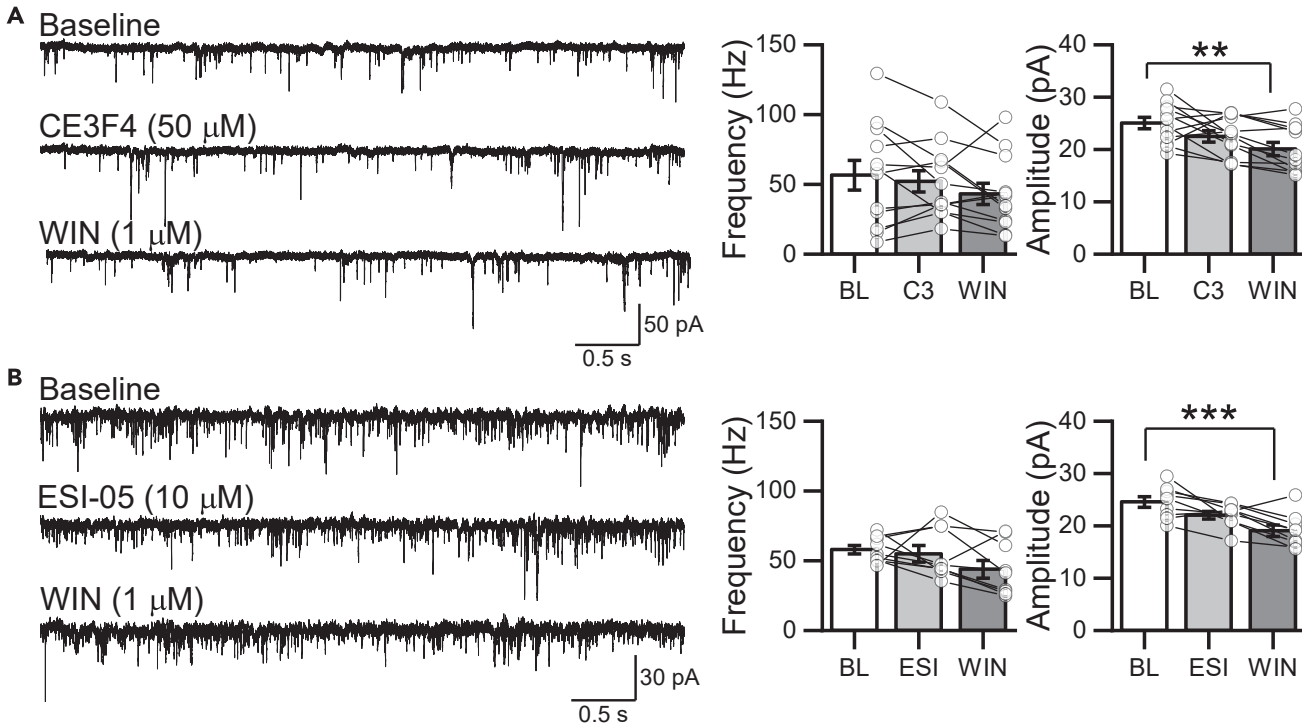

Figure 5. CB1R-mediated effects at RBC terminals require EPAC1/2 signal pathway

(A) Representative traces *(left)* and summarized graph *(right)* showing the effect of the bath application of the EPAC1 inhibitor CE3F4 (50 μM) and subsequent application of WIN (1 μM). Note that CE3F4 did not affect sEPSC frequency or amplitude but eliminated the WIN-mediated decrease of sEPSC frequency and amplitude in AII ACs (n = 12 cells/7 animals, *right*).

(B) Similarly, bath application of the EPAC2 inhibitor ESI-05 (10 μM) also had no effect on sEPSC frequency or amplitude but eliminated the WIN-mediated decrease of sEPSC frequency and amplitude in AII ACs (n = 9 cells/7 animals). Data are presented as mean ± S.E.M and open circles represent a single cell. **p < 0.01, ***p < 0.001. Multiple comparisons were made using one-way ANOVA-RM, followed by a post-hoc Tukey test, or using Friedman ANOVA followed by a post-hoc WMNT test. For statistics, see Table S1.

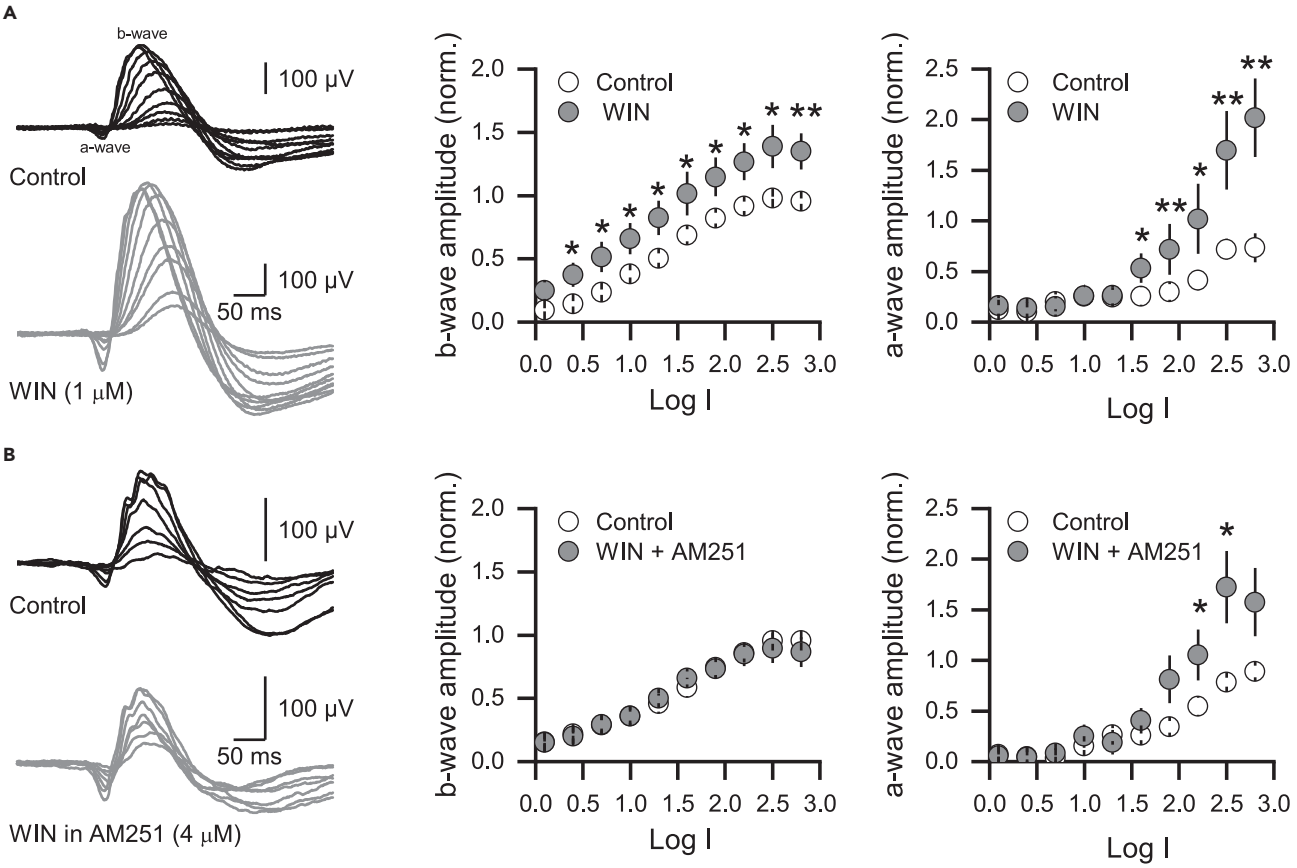

Figure 6. Activation of CB1 receptor enhances scotopic ERG wave amplitudes in the rat retina

(A) ERG sample traces before *(left, top)* and after the intravitreal injection of WIN (1 μM, *n* = 8 animals, *left, bottom*). CB1R activation increased b-wave amplitude independently of light intensity (*middle*), while a-wave amplitude increased only during high light intensity stimulation (*right*).

(B) ERG sample traces before and after the co-application of WIN and AM251 (4 μM, *n* = 9 animals, *left*). Note that the co-application of WIN and AM251 eliminated the WIN-mediated effects on the ERG b-wave (*middle*) but did not prevent the increase in the ERG a-wave (*right*). Data are presented as mean ± S.E.M and open circles represent a single animal. *$p < 0.05$. Comparisons were made using paired t-tests or Wilcoxon signed-rank tests. For statistics, see Table S1.

from RBCs (Figure 5), suggesting that EPAC1/2 play a key role in shaping visual processing and highlight a non-canonical pathway by which CB1R might regulate ribbon synapses. Interestingly, EPAC1/2 promotes the assembly of the Rab3A–RIM1α–Munc13-1 module through the activation of phospholipase C (PLC)[81] or protein kinase C (PKC),[49,52] facilitating the docking and release of synaptic vesicles. Notably, PKCα is not only one of the principal markers of RBCs,[82] but it also plays a role in increasing the pool of synaptic vesicles in bipolar cells of goldfish retina[83] and is essential for the activation and termination of RBC light responses.[84,85] Additional work is necessary to fully understand whether EPAC signaling recruits PKCα to modulate synaptic vesicles at RBC terminals and whether EPAC is a common pathway involved in the modulation of ribbon synapses at sensory systems by CB1R activation.

Type 1 cannabinoid receptors activation impacts rod-driven response *in vivo*

Previous evidence indicates that scotopic ERG b-wave is shaped by reciprocal inhibition, as injections of GABA receptor antagonists significantly increase the amplitude and duration of the scotopic b-wave.[29,86] Given that CB1R activation strongly reduces reciprocal feedback inhibition onto RBC at the single cell level (Figure 2), it was not surprising that injections of WIN also enhanced and prolonged the time course of the ERG b-wave *in vivo* (Figures 6 and 7). Consistent with the role of GABAergic inhibition on the ERG b-wave, all the effects induced by WIN were eliminated in the presence of GABA receptor antagonists (Figures 7B and 7C), strongly suggesting that the effects on ERG b-wave mediated by CB1R activation are likely due to reduced inhibitory feedback onto the RBC terminals, secondary to reduced RBC glutamate release. An alternative scenario is that the increase in the scotopic ERG b-wave amplitude could result from increased rod photoreceptor activity. However, our results argue against this possibility as the increase in the ERG a-wave mediated by WIN occurs only at high light intensity and is unaffected when CB1Rs are blocked (Figure 1B). In contrast, the WIN-mediated increase in the ERG b-wave was light-independent and the change in the temporal properties occurred only at dim-light stimuli (Figure 7), supporting the idea that RBC activity is regulated

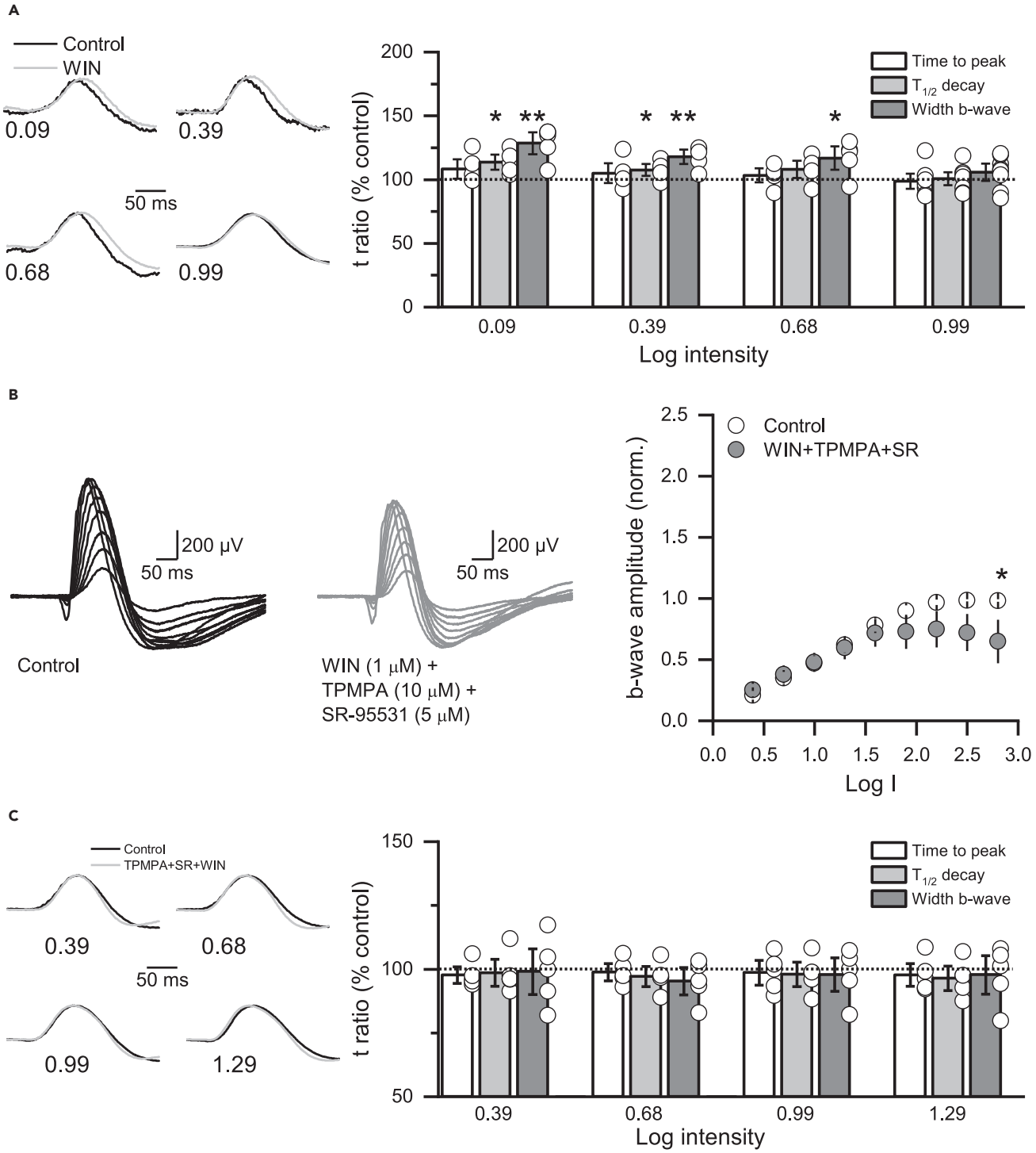

Figure 7. CB1 receptor activation prolongs dim-light ERG b-wave in a GABAR-dependent manner

(A) Normalized ERG b-waves recorded at dim light intensities (*left*) and summary graph (*right*) showing that WIN (1 µM) prolongs the decay time course of the b-wave at dim light intensities (n = 8 animals).

(B) ERG sample traces before (*black*) and after the intravitreal injection of a cocktail of WIN and GABAR antagonists TPMPA (10 µM) and SR95531 (5 µM, *gray*). Note that when both $GABA_A$ and $GABA_C$ receptor blockers where co-applied, WIN no longer affected the amplitude of the ERG b-wave (*right*).

(C) Blocking GABA receptors eliminated the changes in the ERG b-wave kinetics (n = 5 animals). Data are presented as mean ± S.E.M and open circles represent a single animal. *$p < 0.05$, **$p < 0.01$. Comparisons were made using Paired t-tests or Wilcoxon signed-rank tests. For statistics, see Table S1.

by CB1Rs. Interestingly, the observation that WIN enhances the ERG a-wave in a CB1R-independent manner suggests that WIN might have off-target effects at the photoreceptor-bipolar cell synapse. For instance, the activation of the GPR55 is known to play a role in regulating scotopic vision in vervet monkeys.[62] Moreover, CB2R expression has also been reported in rod and cone-type photoreceptors of the mouse retina.[60] Future studies are necessary to determine if these effects on the a-wave amplitude are mediated by CB1Rs and/or CB2R/GPR55. If that is the case, the contribution of each receptor in regulating rod-photoreceptor-bipolar cell synapse should be investigated. Altogether, our findings provide new insights into the mechanism by which CB1Rs regulate night microcircuit in the inner rat retina, providing evidence of functional consequences on dim-light visual response that might help to explain some of the effects of the consumption of marijuana on visual perception at the retinal level.

Limitations of the study

Our study demonstrates that exogenous CB1R activation reduces glutamatergic feedforward and GABAergic feedback signaling at the RBC dyad synapse, modulating rod-driven responses *in vivo*. However, how and under which circumstances endocannabinoids are released to regulate night vision remains unknown. Although our findings demonstrated that CB1R modulate glutamate transmitter release at rod bipolar cells terminals, we cannot rule out the possibility that CB1Rs expressed at photoreceptor levels and/or in postsynaptic amacrine cells could also play a role in regulating visual signal.

STAR★METHODS

Detailed methods are provided in the online version of this paper and include the following:

- KEY RESOURCES TABLE
- RESOURCE AVAILABILITY
  - Lead contact
  - Materials availability
  - Data and code availability
- EXPERIMENTAL MODEL AND STUDY PARTICIPANT DETAILS
- METHOD DETAILS
  - Acute rat retinal slice preparation
  - Electrophysiology recordings
  - Two-photon calcium imaging/Image analysis
  - *In vivo* electroretinogram recordings
- QUANTIFICATION AND STATISTICAL ANALYSIS

SUPPLEMENTAL INFORMATION

Supplemental information can be found online at https://doi.org/10.1016/j.isci.2024.109920.

ACKNOWLEDGMENTS

This work was supported by the Chilean government through FONDECYT grant #1201848 (to A.E.C), # 1171840 (C.Q.C), Fondequip # EQM160154 (A.E.C), and by ANID Millennium Science Initiative Program (ACE210014 to C.Q.C and A.E.C). S.F.E. was supported by PhD fellowship from ANID (21191436).

AUTHOR CONTRIBUTIONS

S.F.E, designed and performed all slices electrophysiological experiments and analyzed the results. C.M.M. performed two photon experiments and analyzed the results. A.H.V and A.P.M performed *in vivo* ERG experiments and analyzed the results. A.E.C and C.Q.C designed experiments, guided the research, provided resources, and interpreted all the results. S.F.E, C.Q.C, and A.E.C wrote and edited the article.

DECLARATION OF INTERESTS

The authors declare no competing financial interests.

Received: February 28, 2024
Revised: April 18, 2024
Accepted: May 3, 2024
Published: May 7, 2024

REFERENCES

1. Herkenham, M., Lynn, A.B., Little, M.D., Johnson, M.R., Melvin, L.S., De Costa, B.R., and Rice, K.C. (1990). Cannabinoid receptor localization in brain. Proc. Natl. Acad. Sci. USA *87*, 1932–1936.
2. Castillo, P.E., Younts, T.J., Chávez, A.E., and Hashimotodani, Y. (2012). Endocannabinoid signaling and synaptic function. Neuron *76*, 70–81. https://doi.org/10.1016/j.neuron.2012.09.020.
3. Katona, I., and Freund, T.F. (2012). Multiple functions of endocannabinoid signaling in the brain. Annu. Rev. Neurosci. *35*, 529–558. https://doi.org/10.1146/annurev-neuro-062111-150420.
4. Heinbockel, T., and Straiker, A. (2021). Cannabinoids Regulate Sensory Processing in Early Olfactory and Visual Neural Circuits. Front. Neural Circ. *15*, 662349. https://doi.org/10.3389/fncir.2021.662349.
5. Marsicano, G., and Lafenêtre, P. (2009). Roles of the endocannabinoid system in learning and memory. Curr. Top. Behav. Neurosci. *1*, 201–230. https://doi.org/10.1007/978-3-540-88955-7_8.
6. Zabouri, N., Bouchard, J.F., and Casanova, C. (2011). Cannabinoid receptor type 1 expression during postnatal development of the rat retina. J. Comp. Neurol. *519*, 1258–1280. https://doi.org/10.1002/cne.22534.
7. Yazulla, S., Studholme, K.M., McIntosh, H.H., and Deutsch, D.G. (1999). Immunocytochemical localization of cannabinoid CB1 receptor and fatty acid amide hydrolase in rat retina. J. Comp. Neurol. *415*, 80–90.
8. Straiker, A.J., Maguire, G., Mackie, K., and Lindsey, J. (1999). Localization of cannabinoid CB1 receptors in the human anterior eye and retina. Invest. Ophthalmol. Vis. Sci. *40*, 2442–2448.
9. Bouskila, J., Burke, M.W., Zabouri, N., Casanova, C., Ptito, M., and Bouchard, J.F. (2012). Expression and localization of the cannabinoid receptor type 1 and the enzyme fatty acid amide hydrolase in the retina of vervet monkeys. Neuroscience *202*, 117–130. https://doi.org/10.1016/j.neuroscience.2011.11.041.
10. Straiker, A., Stella, N., Piomelli, D., Mackie, K., Karten, H.J., and Maguire, G. (1999). Cannabinoid CB1 receptors and ligands in vertebrate retina: localization and function of an endogenous signaling system. Proc. Natl. Acad. Sci. USA *96*, 14565–14570.
11. Middleton, T.P., and Protti, D.A. (2011). Cannabinoids modulate spontaneous synaptic activity in retinal ganglion cells. Vis. Neurosci. *28*, 393–402. https://doi.org/10.1017/S0952523811000198.
12. Middleton, T.P., Huang, J.Y., and Protti, D.A. (2019). Cannabinoids Modulate Light Signaling in ON-Sustained Retinal Ganglion Cells of the Mouse. Front. Neural Circ. *13*, 37. https://doi.org/10.3389/fncir.2019.00037.
13. Vielma, A.H., Tapia, F., Alcaino, A., Fuenzalida, M., Schmachtenberg, O., and Chávez, A.E. (2020). Cannabinoid Signaling Selectively Modulates GABAergic Inhibitory Input to OFF Bipolar Cells in Rat Retina. Invest. Ophthalmol. Vis. Sci. *61*, 3. https://doi.org/10.1167/iovs.61.3.3.
14. Yates, C.F., Huang, J.Y., and Protti, D.A. (2022). Tonic Endocannabinoid Levels Modulate Retinal Signaling. Int. J. Environ. Res. Publ. Health *19*, 12460. https://doi.org/10.3390/ijerph191912460.
15. Wang, X.H., Wu, Y., Yang, X.F., Miao, Y., Zhang, C.Q., Dong, L.D., Yang, X.L., and Wang, Z. (2016). Cannabinoid CB1 receptor signaling dichotomously modulates inhibitory and excitatory synaptic transmission in rat inner retina. Brain Struct. Funct. *221*, 301–316. https://doi.org/10.1007/s00429-014-0908-4.
16. West, M.E. (1991). Cannabis and night vision. Nature *351*, 703–704. https://doi.org/10.1038/351703b0.
17. Dawson, W.W., Jiménez-Antillon, C.F., Perez, J.M., Zeskind, J.A., and Science, V. (1977). Marijuana and vision-after ten years' use in Costa Rica. Invest. Ophthalmol. Vis. Sci. *16*, 689–699.
18. Consroe, P., Musty, R., Rein, J., Tillery, W., and Pertwee, R. (1997). The perceived effects of smoked cannabis on patients with multiple sclerosis. Eur. Neurol. *38*, 44–48.
19. Russo, E.B., Merzouki, A., Mesa, J.M., Frey, K.A., and Bach, P.J. (2004). Cannabis improves night vision: a case study of dark adaptometry and scotopic sensitivity in kif smokers of the Rif mountains of northern Morocco. J. Ethnopharmacol. *93*, 99–104. https://doi.org/10.1016/j.jep.2004.03.029.
20. Merzouki, A., and Mesa, J.M. (2002). Concerning kif, a Cannabis sativa L. preparation smoked in the Rif mountains of northern Morocco. J. Ethnopharmacol. *81*, 403–406. https://doi.org/10.1016/s0378-8741(02)00119-8.
21. Miraucourt, L.S., Tsui, J., Gobert, D., Desjardins, J.F., Schohl, A., Sild, M., Spratt, P., Castonguay, A., De Koninck, Y., Marsh-Armstrong, N., et al. (2016). Endocannabinoid signaling enhances visual responses through modulation of intracellular chloride levels in retinal ganglion cells. Elife *5*, e15932. https://doi.org/10.7554/eLife.15932.
22. Famiglietti, E.V., and Kolb, H. (1975). A bistratified amacrine cell and synaptic circuitry in the inner plexiform layer of the retina. Brain Res. *84*, 293–300. https://doi.org/10.1016/0006-8993(75)90983-x.
23. Dacheux, R.F., and Raviola, E. (1986). The rod pathway in the rabbit retina: a depolarizing bipolar and amacrine cell. J. Neurosci. *6*, 331–345. https://doi.org/10.1523/JNEUROSCI.06-02-00331.
24. Graydon, C.W., Lieberman, E.E., Rho, N., Briggman, K.L., Singer, J.H., and Diamond, J.S. (2018). Synaptic Transfer between Rod and Cone Pathways Mediated by AII Amacrine Cells in the Mouse Retina. Curr. Biol. *28*, 2739–2751.e3. https://doi.org/10.1016/j.cub.2018.06.063.
25. Hartveit, E. (1999). Reciprocal synaptic interactions between rod bipolar cells and amacrine cells in the rat retina. J. Neurophysiol. *81*, 2923–2936. https://doi.org/10.1152/jn.1999.81.6.2923.
26. Kolb, H., and Nelson, R. (1983). Rod pathways in the retina of the cat. Vis. Res. *23*, 301–312. https://doi.org/10.1016/0042-6989(83)90078-0.
27. Raviola, E., and Dacheux, R.F. (1987). Excitatory dyad synapse in rabbit retina. Proc. Natl. Acad. Sci. USA *84*, 7324–7328. https://doi.org/10.1073/pnas.84.20.7324.
28. Chavez, A.E., Singer, J.H., and Diamond, J.S. (2006). Fast neurotransmitter release triggered by Ca influx through AMPA-type glutamate receptors. Nature *443*, 705–708. https://doi.org/10.1038/nature05123.
29. Dong, C.J., and Hare, W.A. (2003). Temporal modulation of scotopic visual signals by A17 amacrine cells in mammalian retina *in vivo*. J. Neurophysiol. *89*, 2159–2166. https://doi.org/10.1152/jn.01008.2002.
30. Chavez, A.E., and Diamond, J.S. (2008). Diverse mechanisms underlie glycinergic feedback transmission onto rod bipolar cells in rat retina. J. Neurosci. *28*, 7919–7928. https://doi.org/10.1523/JNEUROSCI.0784-08.2008.
31. Chavez, A.E., Grimes, W.N., and Diamond, J.S. (2010). Mechanisms underlying lateral GABAergic feedback onto rod bipolar cells in rat retina. J. Neurosci. *30*, 2330–2339. https://doi.org/10.1523/JNEUROSCI.5574-09.2010.
32. Volgyi, B., Xin, D., and Bloomfield, S.A. (2002). Feedback inhibition in the inner plexiform layer underlies the surround-mediated responses of AII amacrine cells in the mammalian retina. J. Physiol. *539*, 603–614. https://doi.org/10.1013/jphysiol.2001.013133.
33. Cui, J., Ma, Y.P., Lipton, S.A., and Pan, Z.H. (2003). Glycine receptors and glycinergic synaptic input at the axon terminals of mammalian retinal rod bipolar cells. J. Physiol. *553*, 895–909. https://doi.org/10.1113/jphysiol.2003.052092.
34. Eggers, E.D., and Lukasiewicz, P.D. (2006). Receptor and transmitter release properties set the time course of retinal inhibition. J. Neurosci. *26*, 9413–9425. https://doi.org/10.1523/JNEUROSCI.2591-06.2006.
35. Eggers, E.D., and Lukasiewicz, P.D. (2006). GABA(A), GABA(C) and glycine receptor-mediated inhibition differentially affects light-evoked signalling from mouse retinal rod bipolar cells. J. Physiol. *572*, 215–225. https://doi.org/10.1113/jphysiol.2005.103648.
36. Eggers, E.D., McCall, M.A., and Lukasiewicz, P.D. (2007). Presynaptic inhibition differentially shapes transmission in distinct circuits in the mouse retina. J. Physiol. *582*, 569–582. https://doi.org/10.1113/jphysiol.2007.131763.
37. Ivanova, E., Müller, U., and Wässle, H. (2006). Characterization of the glycinergic input to bipolar cells of the mouse retina. Eur. J. Neurosci. *23*, 350–364. https://doi.org/10.1111/j.1460-9568.2005.04557.x.
38. Moller, A., and Eysteinsson, T. (2003). Modulation of the components of the rat dark-adapted electroretinogram by the three subtypes of GABA receptors. Vis. Neurosci. *20*, 535–542. https://doi.org/10.1017/s0952523803205071.
39. Straiker, A., and Sullivan, J.M. (2003). Cannabinoid receptor activation differentially modulates ion channels in photoreceptors of the tiger salamander. J. Neurophysiol. *89*, 2647–2654. https://doi.org/10.1152/jn.00268.2002.
40. Felder, C.C., Joyce, K.E., Briley, E.M., Mansouri, J., Mackie, K., Blond, O., Lai, Y., Ma, A.L., and Mitchell, R.L. (1995). Comparison of the pharmacology and signal transduction of the human cannabinoid CB1 and CB2 receptors. Mol. Pharmacol. *48*, 443–450.
41. Lalonde, M.R., Jollimore, C.A.B., Stevens, K., Barnes, S., and Kelly, M.E.M. (2006). Cannabinoid receptor-mediated inhibition of calcium signaling in rat retinal ganglion cells. Mol. Vis. *12*, 1160–1166.

42. Soto, F., Lambrecht, G., Nickel, P., Stühmer, W., and Busch, A.E. (1999). Antagonistic properties of the suramin analogue NF023 at heterologously expressed P2X receptors. Neuropharmacology *38*, 141–149. https://doi.org/10.1016/s0028-3908(98)00158-0.
43. Chavez-Noriega, L.E., and Stevens, C.F. (1994). Increased transmitter release at excitatory synapses produced by direct activation of adenylate cyclase in rat hippocampal slices. J. Neurosci. *14*, 310–317. https://doi.org/10.1523/JNEUROSCI.14-01-00310.1994.
44. Pelkey, K.A., Topolnik, L., Yuan, X.Q., Lacaille, J.C., and McBain, C.J. (2008). State-dependent cAMP sensitivity of presynaptic function underlies metaplasticity in a hippocampal feedforward inhibitory circuit. Neuron *60*, 980–987. https://doi.org/10.1016/j.neuron.2008.11.018.
45. Salin, P.A., Malenka, R.C., and Nicoll, R.A. (1996). Cyclic AMP Mediates a Presynaptic Form of LTP at Cerebellar Parallel Fiber Synapses. Neuron *16*, 797–803. https://doi.org/10.1016/s0896-6273(00)80099-9.
46. Weisskopf, M.G., Castillo, P.E., Zalutsky, R.A., and Nicoll, R.A. (1994). Mediation of hippocampal mossy fiber long-term potentiation by cyclic AMP. Science *265*, 1878–1882. https://doi.org/10.1126/science.7916482.
47. de Rooij, J., Zwartkruis, F.J., Verheijen, M.H., Cool, R.H., Nijman, S.M., Wittinghofer, A., and Bos, J.L. (1998). Epac is a Rap1 guanine-nucleotide-exchange factor directly activated by cyclic AMP. Nature *396*, 474–477. https://doi.org/10.1038/24884.
48. Kawasaki, H., Springett, G.M., Mochizuki, N., Toki, S., Nakaya, M., Matsuda, M., Housman, D.E., and Graybiel, A.M. (1998). A family of cAMP-binding proteins that directly activate Rap1. Science *282*, 2275–2279. https://doi.org/10.1126/science.282.5397.2275.
49. Gekel, I., and Neher, E. (2008). Application of an Epac activator enhances neurotransmitter release at excitatory central synapses. J. Neurosci. *28*, 7991–8002. https://doi.org/10.1523/JNEUROSCI.0268-08.2008.
50. Woolfrey, K.M., Srivastava, D.P., Photowala, H., Yamashita, M., Barbolina, M.V., Cahill, M.E., Xie, Z., Jones, K.A., Quilliam, L.A., Prakriya, M., and Penzes, P. (2009). Epac2 induces synapse remodeling and depression and its disease-associated forms alter spines. Nat. Neurosci. *12*, 1275–1284. https://doi.org/10.1038/nn.2386.
51. Fernandes, H.B., Riordan, S., Nomura, T., Remmers, C.L., Kraniotis, S., Marshall, J.J., Kukreja, L., Vassar, R., and Contractor, A. (2015). Epac2 Mediates cAMP-Dependent Potentiation of Neurotransmission in the Hippocampus. J. Neurosci. *35*, 6544–6553. https://doi.org/10.1523/JNEUROSCI.0314-14.2015.
52. Wang, X.T., Zhou, L., Dong, B.B., Xu, F.X., Wang, D.J., Shen, E.W., Cai, X.Y., Wang, Y., Wang, N., Ji, S.J., et al. (2023). cAMP-EPAC-PKCepsilon-RIM1alpha signaling regulates presynaptic long-term potentiation and motor learning. Elife *12*, e80875. https://doi.org/10.7554/eLife.80875.
53. Kaneko, M., and Takahashi, T. (2004). Presynaptic mechanism underlying cAMP-dependent synaptic potentiation. J. Neurosci. *24*, 5202–5208. https://doi.org/10.1523/JNEUROSCI.0999-04.2004.
54. Meadows, M.A., Balakrishnan, V., Wang, X., and von Gersdorff, H. (2021). Glycine Release Is Potentiated by cAMP via EPAC2 and Ca(2+) Stores in a Retinal Interneuron. J. Neurosci. *41*, 9503–9520. https://doi.org/10.1523/JNEUROSCI.0670-21.2021.
55. Alonso, B., Bartolomé-Martín, D., Ferrero, J.J., Ramírez-Franco, J., Torres, M., and Sánchez-Prieto, J. (2017). CB1 receptors down-regulate a cAMP/Epac2/PLC pathway to silence the nerve terminals of cerebellar granule cells. J. Neurochem. *142*, 350–364. https://doi.org/10.1111/jnc.14059.
56. Ramirez-Franco, J., Bartolome-Martin, D., Alonso, B., Torres, M., and Sanchez-Prieto, J. (2014). Cannabinoid type 1 receptors transiently silence glutamatergic nerve terminals of cultured cerebellar granule cells. PLoS One *9*, e88594. https://doi.org/10.1371/journal.pone.0088594.
57. Sartre, C., Peurois, F., Ley, M., Kryszke, M.H., Zhang, W., Courilleau, D., Fischmeister, R., Ambroise, Y., Zeghouf, M., Cianferani, S., et al. (2023). Membranes prime the RapGEF EPAC1 to transduce cAMP signaling. Nat. Commun. *14*, 4157. https://doi.org/10.1038/s41467-023-39894-4.
58. Courilleau, D., Bisserier, M., Jullian, J.C., Lucas, A., Bouyssou, P., Fischmeister, R., Blondeau, J.P., and Lezoualc'h, F. (2012). Identification of a tetrahydroquinoline analog as a pharmacological inhibitor of the cAMP-binding protein Epac. J. Biol. Chem. *287*, 44192–44202. https://doi.org/10.1074/jbc.M112.422956.
59. Tsalkova, T., Mei, F.C., Li, S., Chepurny, O.G., Leech, C.A., Liu, T., Holz, G.G., Woods, V.L., Jr., and Cheng, X. (2012). Isoform-specific antagonists of exchange proteins directly activated by cAMP. Proc. Natl. Acad. Sci. USA *109*, 18613–18618. https://doi.org/10.1073/pnas.1210209109.
60. Cecyre, B., Zabouri, N., Huppe-Gourgues, F., Bouchard, J.F., and Casanova, C. (2013). Roles of cannabinoid receptors type 1 and 2 on the retinal function of adult mice. Invest. Ophthalmol. Vis. Sci. *54*, 8079–8090. https://doi.org/10.1167/iovs.13-12514.
61. Bouskila, J., Harrar, V., Javadi, P., Beierschmitt, A., Palmour, R., Casanova, C., Bouchard, J.F., and Ptito, M. (2016). Cannabinoid Receptors CB1 and CB2 Modulate the Electroretinographic Waves in Vervet Monkeys. Neural Plast. *2016*, 1253245. https://doi.org/10.1155/2016/1253245.
62. Bouskila, J., Harrar, V., Javadi, P., Casanova, C., Hirabayashi, Y., Matsuo, I., Ohyama, J., Bouchard, J.F., and Ptito, M. (2016). Scotopic vision in the monkey is modulated by the G protein-coupled receptor 55. Vis. Neurosci. *33*, E006. https://doi.org/10.1017/S095252381600002X.
63. Euler, T., and Masland, R.H. (2000). Light-evoked responses of bipolar cells in a mammalian retina. J. Neurophysiol. *83*, 1817–1829. https://doi.org/10.1152/jn.2000.83.4.1817.
64. Eggers, E.D., and Lukasiewicz, P.D. (2011). Multiple pathways of inhibition shape bipolar cell responses in the retina. Vis. Neurosci. *28*, 95–108. https://doi.org/10.1017/S0952523810000209.
65. Hu, S.S.J., Arnold, A., Hutchens, J.M., Radicke, J., Cravatt, B.F., Wager-Miller, J., Mackie, K., and Straiker, A. (2010). Architecture of cannabinoid signaling in mouse retina. J. Comp. Neurol. *518*, 3848–3866. https://doi.org/10.1002/cne.22429.
66. Borowska-Fielding, J., Murataeva, N., Smith, B., Szczesniak, A.M., Leishman, E., Daily, L., Toguri, J.T., Hillard, C.J., Romero, J., Bradshaw, H., et al. (2018). Revisiting cannabinoid receptor 2 expression and function in murine retina. Neuropharmacology *141*, 21–31. https://doi.org/10.1016/j.neuropharm.2018.08.007.
67. Jordan, C.J., and Xi, Z.X. (2019). Progress in brain cannabinoid CB(2) receptor research: From genes to behavior. Neurosci. Biobehav. Rev. *98*, 208–220. https://doi.org/10.1016/j.neubiorev.2018.12.026.
68. Lu, Q., Straiker, A., Lu, Q., and Maguire, G. (2000). Expression of CB2 cannabinoid receptor mRNA in adult rat retina. Vis. Neurosci. *17*, 91–95. https://doi.org/10.1017/s0952523800171093.
69. Lopez, E.M., Tagliaferro, P., Onaivi, E.S., and Lopez-Costa, J.J. (2011). Distribution of CB2 cannabinoid receptor in adult rat retina. Synapse *65*, 388–392. https://doi.org/10.1002/syn.20856.
70. Agler, H.L., Evans, J., Colecraft, H.M., and Yue, D.T. (2003). Custom distinctions in the interaction of G-protein beta subunits with N-type (CaV2.2) versus P/Q-type (CaV2.1) calcium channels. J. Gen. Physiol. *121*, 495–510. https://doi.org/10.1085/jgp.200208770.
71. Roloff, A.M., and Thayer, S.A. (2009). Modulation of excitatory synaptic transmission by Delta 9-tetrahydrocannabinol switches from agonist to antagonist depending on firing rate. Mol. Pharmacol. *75*, 892–900. https://doi.org/10.1124/mol.108.051482.
72. Jensen, K.R., Berthoux, C., Nasrallah, K., and Castillo, P.E. (2021). Multiple cannabinoid signaling cascades powerfully suppress recurrent excitation in the hippocampus. Proc. Natl. Acad. Sci. USA *118*, e2017590118. https://doi.org/10.1073/pnas.2017590118.
73. Winters, B.L., and Vaughan, C.W. (2021). Mechanisms of endocannabinoid control of synaptic plasticity. Neuropharmacology *197*, 108736. https://doi.org/10.1016/j.neuropharm.2021.108736.
74. Lovinger, D.M. (2008). Presynaptic modulation by endocannabinoids. Handb. Exp. Pharmacol. 435–477. https://doi.org/10.1007/978-3-540-74805-2_14.
75. Kano, M., Ohno-Shosaku, T., Hashimotodani, Y., Uchigashima, M., and Watanabe, M. (2009). Endocannabinoid-mediated control of synaptic transmission. Physiol. Rev. *89*, 309–380. https://doi.org/10.1152/physrev.00019.2008.
76. Cheng, X., Ji, Z., Tsalkova, T., and Mei, F. (2008). Epac and PKA: a tale of two intracellular cAMP receptors. Acta Biochim. Biophys. Sin. *40*, 651–662. https://doi.org/10.1111/j.1745-7270.2008.00438.x.
77. Lee, K. (2021). Epac: new emerging cAMP-binding protein. BMB Rep. *54*, 149–156. https://doi.org/10.5483/BMBRep.2021.54.3.233.
78. Seino, S., and Shibasaki, T. (2005). PKA-dependent and PKA-independent pathways for cAMP-regulated exocytosis. Physiol. Rev. *85*, 1303–1342. https://doi.org/10.1152/physrev.00001.2005.
79. Whitaker, C.M., and Cooper, N.G.F. (2010). Differential distribution of exchange proteins directly activated by cyclic AMP within the adult rat retina. Neuroscience *165*, 955–967. https://doi.org/10.1016/j.neuroscience.2009.10.054.
80. Kantardzhieva, A., Peppi, M., Lane, W.S., and Sewell, W.F. (2012). Protein composition of immunoprecipitated synaptic ribbons. J. Proteome Res. *11*, 1163–1174. https://doi.org/10.1021/pr2008972.

81. Ferrero, J.J., Alvarez, A.M., Ramírez-Franco, J., Godino, M.C., Bartolomé-Martín, D., Aguado, C., Torres, M., Luján, R., Ciruela, F., and Sánchez-Prieto, J. (2013). beta-Adrenergic receptors activate exchange protein directly activated by cAMP (Epac), translocate Munc13-1, and enhance the Rab3A-RIM1alpha interaction to potentiate glutamate release at cerebrocortical nerve terminals. J. Biol. Chem. *288*, 31370–31385. https://doi.org/10.1074/jbc.M113.463877.

82. Greferath, U., Grünert, U., and Wässle, H. (1990). Rod bipolar cells in the mammalian retina show protein kinase C-like immunoreactivity. J. Comp. Neurol. *301*, 433–442. https://doi.org/10.1002/cne.903010308.

83. Berglund, K., Midorikawa, M., and Tachibana, M. (2002). Increase in the pool size of releasable synaptic vesicles by the activation of protein kinase C in goldfish retinal bipolar cells. J. Neurosci. *22*, 4776–4785. https://doi.org/10.1523/JNEUROSCI.22-12-04776.2002.

84. Ruether, K., Feigenspan, A., Pirngruber, J., Leitges, M., Baehr, W., and Strauss, O. (2010). PKCalpha is essential for the proper activation and termination of rod bipolar cell response. Invest. Ophthalmol. Vis. Sci. *51*, 6051–6058. https://doi.org/10.1167/iovs.09-4704.

85. Xiong, W.H., Pang, J.J., Pennesi, M.E., Duvoisin, R.M., Wu, S.M., and Morgans, C.W. (2015). The Effect of PKCalpha on the Light Response of Rod Bipolar Cells in the Mouse Retina. Invest. Ophthalmol. Vis. Sci. *56*, 4961–4974. https://doi.org/10.1167/iovs.15-16622.

86. Dong, C.J., and Hare, W.A. (2002). GABAc feedback pathway modulates the amplitude and kinetics of ERG b-wave in a mammalian retina *in vivo*. Vis. Res. *42*, 1081–1087.

87. Schindelin, J., Arganda-Carreras, I., Frise, E., Kaynig, V., Longair, M., Pietzsch, T., Preibisch, S., Rueden, C., Saalfeld, S., Schmid, B., et al. (2012). Fiji: an open-source platform for biological-image analysis. Nat. Methods *9*, 676–682. https://doi.org/10.1038/nmeth.2019.

88. Demb, J.B., and Singer, J.H. (2012). Intrinsic properties and functional circuitry of the AII amacrine cell. Vis. Neurosci. *29*, 51–60. https://doi.org/10.1017/S0952523811000368.

89. Menger, N., and Wässle, H. (2000). Morphological and physiological properties of the A17 amacrine cell of the rat retina. Vis. Neurosci. *17*, 769–780.

90. Singer, J.H., and Diamond, J.S. (2003). Sustained Ca2+ entry elicits transient postsynaptic currents at a retinal ribbon synapse. J. Neurosci. *23*, 10923–10933.

91. Grimes, W.N., Zhang, J., Graydon, C.W., Kachar, B., and Diamond, J.S. (2010). Retinal parallel processors: more than 100 independent microcircuits operate within a single interneuron. Neuron *65*, 873–885. https://doi.org/10.1016/j.neuron.2010.02.028.

92. Grimes, W.N., Zhang, J., Tian, H., Graydon, C.W., Hoon, M., Rieke, F., and Diamond, J.S. (2015). Complex inhibitory microcircuitry regulates retinal signaling near visual threshold. J. Neurophysiol. *114*, 341–353. https://doi.org/10.1152/jn.00017.2015.

93. Chávez, A.E., Roncagliolo, M., Kuhrt, H., Reichenbach, A., and Palacios, A.G. (2003). The retinal anatomy and function of the myelin mutant taiep rat. Brain Res. *964*, 144–152. https://doi.org/10.1016/s0006-8993(02)04114-8.

94. Naarendorp, F., and Williams, G.E. (1999). The d-wave of the rod electroretinogram of rat originates in the cone pathway. Vis. Neurosci. *16*, 91–105.

95. Green, D.G., and Kapousta-Bruneau, N.V. (1999). A dissection of the electroretinogram from the isolated rat retina with microelectrodes and drugs. Vis. Neurosci. *16*, 727–741.

96. Stockton, R.A., and Slaughter, M.M. (1989). B-wave of the electroretinogram. A reflection of ON bipolar cell activity. J. Gen. Physiol. *93*, 101–122.

STAR★METHODS

KEY RESOURCES TABLE

REAGENT or RESOURCE	SOURCE	IDENTIFIER
Chemicals, peptides, and recombinant proteins		
Ketamine hydrochloride (Ketamil)	Ilium, Troy Laboratories	Cat#:170366 CAS: 1867-66-9
Xylazine 2% (Xylavet)	Alfasan B.V.	Cat#1608238-04 CAS: 23076-35-9
Lidocaine hydrochloride 2%	Fresenius Kabi	Cat#920102 CAS: 6108-05-0
Atropine sulfate	Biosano laboratorio	Cat#:17.01.0693 CAS: 55-48-1
Isoflurane	Baxter	Cat#218-082 CAS: 26675-46-7
Dimethyl sulfoxide (DMSO)	Sigma-Aldrich	Cat#D84180; CAS:67-68-5
NaCl	Sigma-Aldrich	Cat#S7653; CAS:7647-14-5
$NaHCO_3$	Merck	Cat#106329; CAS:144-55-8 55-8
Na_2HPO_4	Sigma-Aldrich	Cat#S0751; CAS:7558-80-7
KCl	Sigma-Aldrich	Cat#P4504; CAS: 7447-40-7
$CaCl_2$	Honeywell (Fluka)	Cat#21114; CAS: 10043-52-4
$MgSO_4$ heptahydrate	Sigma-Aldrich	Cat#230391; CAS: 10034-99-8
$MgCl_2$	Honeywell (Fluka)	Cat#63020; CAS:7786-30-3
D-Glucose	Sigma-Aldrich	Cat#G8270; CAS:50-99-7
Sodium pyruvate	Sigma-Aldrich	Cat#P2256; CAS:113-24-6
Sodium L-lactate	Sigma-Aldrich	Cat#71718; CAS:867-56-1
NaOH	Sigma-Aldrich	Cat#S5881; CAS:1310-73-2
CsOH	Sigma-Aldrich	Cat#232041; CAS:21351-79-1
KOH	Sigma-Aldrich	Cat#P1767 CAS: 1310-58-3
Low-melting point agarose	Merck	Cat# 2070-OP; CAS: 9012-36-6
Cesium methanesulfonate	Sigma-Aldrich	Cat#C1426; CAS:2550-61-0
Potassium methanesulfonate	Sigma-Aldrich	Cat#83000;CAS: 2386-56-3
Tetraethylammonium chloride (TEA-Cl)	Sigma-Aldrich	Cat#T2265; CAS:56-34-8
HEPES	Sigma-Aldrich	Cat#H3375; CAS:7365-45-9
BAPTA Tetrasodium Salt	Merck	Cat# US1196418; CAS:126824-24-6
EGTA	Sigma-Aldrich	Cat#E4378; CAS:7-42-5
Na_2-phosphocreatine	Merck	Cat#2380; CAS:19333-65-4
Mg-ATP	Sigma-Aldrich	Cat#A9187; CAS: 74804-12-9
Na-GTP	Sigma-Aldrich	Cat#G8877: CAS: 36051-31-7
Na_2-ATP	Sigma-Aldrich	CaT#: A7699; CAS: 34369-07-8
L-glutamic acid	Sigma-Aldrich	Cat#G1626; CAS:42-47-2
Alexa Fluor-488 hydrazide	Invitrogen	Cat#A10436
Alexa Fluor-594 hydrazide	Invitrogen	Cat#A10438

(*Continued on next page*)

Continued

REAGENT or RESOURCE	SOURCE	IDENTIFIER
Fluo-5F, Pentapotassium Salt	Invitrogen	Cat#F14221
5,7-dihydroxytryptamine (DHT) hydrobromide	Chemodex	Cat#H0026; CAS:31363-74-3
Tetrodotoxin (TTX) citrate	HelloBio	Cat#HB1035; CAS:18660-81-6
SR 95531 hydrobromide	Tocris	Cat#1262; CAS:104104-50-9
TPMPA	Tocris	Cat#1040; CAS: 182485-36-5
Strychnine hydrochloride	Sigma-Aldrich	Cat#S8753; CAS:1421-86-9
DL-APV	Tocris	Cat#0125; CAS:76326-31-3
(R)-(+)-WIN 55,212-2	Sigma-Aldrich	Cat#W102; CAS:131543-23-2
AM251	Tocris	Cat#1117; CAS:183232-66-8
AM630	Tocris	Cat#1120; CAS:164178-33-0
Gallein	Tocris	Cat#3090; CAS:2103-64-2
NF023	Tocris	Cat#1240; CAS:104869-31-0
Forskolin (FSK)	Tocris	Cat#1099; CAS:66575-29-9
H89 dihydrochloride	Tocris	Cat#2910; CAS:130964-39-5
CE3F4	Sigma-Aldrich	Cat#SML2041; CAS: 143703-25-7
ESI-05	Sigma-Aldrich	Cat#SML1907; CAS:5184-64-5
PPADS tetrasodium salt	Tocris	Cat#0625; CAS:192575-19-2
Experimental models: Organisms/strains		
Rats: Sprague-Dawley (both sexes)	Charles River	https://www.criver.com/products-services/research-models-services/animal-models/rats?region=3616
Software and algorithms		
ImageJ	Schindelin et al.[87]	https://imagej.net/ij/
Mini Analysis Program	Synaptosoft	http://www.synaptosoft.com/MiniAnalysis/
GraphPad Prism 9	Graphpad	https://www.graphpad.com/scientificsoftware/prism/
IgorPro	Wavemetrics	https://www.wavemetrics.com/
OriginPro 9	OriginLab	http://www.originlab.com/
Scanimage	Scientifica	https://www.scientifica.uk.com/products/vidrio-technologies-scanimage
Other		
VT-1200S microslicer	Leica Microsystems Co	VT-1200S
Multiclamp 700B amplifier	Axon Instruments	MultiClamp 700B
Nikon eclipse FN1 microscope	Nikon	EFN1
Picospritzer II	General Valve corporation	Picospritzer II
AC/DC differential amplifier	A-M Systems	Model3000
Two-photon laser-scanning microscope	Scientifica	Hyperscope
Ti-Sapphire laser	Spectra Physics	Mai Tai DeepSee

RESOURCE AVAILABILITY

Lead contact

Further information and requests for resources and reagents should be directed to and will be fulfilled by the lead contact, Andrés E. Chávez (andres.chavez@uv.cl).

Materials availability

This study did not generate new unique reagents.

Data and code availability

- The electrophysiological and imaging datasets collected in this paper will be shared by the lead contact upon request.

- This paper does not report original code.
- Any additional information required to reanalyze the data reported in this paper is available from the lead contact upon request.

EXPERIMENTAL MODEL AND STUDY PARTICIPANT DETAILS

For *ex vivo and in vivo* experiments *Sprague-Dawley* rats postnatal day P30-P45 of either sex were used. Animals were housed at ~20°C with *ad libitum* access to food and water on a 12:12 h light/dark cycle. All experimental procedures were conducted following the bioethics regulations of the Chilean Research Council (ANID) and approved by the bioethics committee of the Universidad de Valparaíso, Chile (BEA159-20, CBC41/2022).

METHOD DETAILS

Acute rat retinal slice preparation

Rat retinal slices were prepared using previously described methods.[13,28,30] Briefly, animals were decapitated following isoflurane anesthesia, eyes were enucleated, the cornea, lens, and vitreous humor were removed, and the retina was isolated at room temperature (RT) in artificial cerebrospinal fluid (ACSF) composed by (in mM): 119 NaCl, 26 $NaHCO_3$, 1,25 Na_2HPO_4, 2,5 KCl, 2,5 $CaCl_2$, 1,5 $MgSO_4$, 10 Glucose, 2 Na-pyruvate and 4 Na-lactate (290-295 mOsm). The ACSF was bubbled with carbogen (95% O2/5% CO2) and the pH was adjusted to 7.4 with NaOH. The retina was cut in halves and a section of ~1mm^2 was embedded in 3% (w/v) low-melting point agarose (in ACSF with $NaHCO_3$ substituted for HEPES (10 mM)). The agar block was mounted and cut in 210 μm sections using a Leica Vibratome VT1200S (Leica Microsystems AG, Wetzlar, Germany). Acute retinal slices were used after a 30 min stabilization period and were maintained for up to 6 hours in ACSF continuously bubbled with carbogen.

Electrophysiology recordings

Retinal slices were transferred to a recording chamber on a fixed-stage Nikon FN1 microscope, visualized using infrared differential interference contrast (DIC) video microscopy and perfused at a rate of 1-2 mL/min with ACSF at 28 ± 1°C. Whole-cell voltage-clamp recordings were made using electrodes with a resistance between 8-10 MΩ for RBCs and 6-8 MΩ for AII-A17 ACs. All experiments were done under low-light conditions (room light). For RBCs, we used a cesium-based intracellular solution composed by (in mM): 100 Cs-methanesulfonate, 20 Tetraethylammonium chloride (TEA-Cl), 10 HEPES, 1.5 BAPTA, 10 Na_2-phosphocreatine, 4 Mg-ATP, 0.4 Na-GTP y 10 L-glutamic acid (~285 mOsm). Intracellular solution for A17 and AII ACs recordings contained (in mM): 100 Cs-methanesulfonate, 20 TEA-Cl, 10 HEPES, 10 EGTA, 10 Na_2-phosphocreatine, 4 Mg-ATP, 0.4 Na-GTP (~285 mOsm). The pH was adjusted to 7.2-7.3 with CsOH. For two-photon experiments, intracellular solution contained (in mM): 125 K-methanesulfonate, 10 HEPES, 1 EGTA, 4 $MgCl_2$, 4 Na_2-ATP, 0.4 Na-GTP and 10 Na_2-phosphocreatine, adjusted to pH 7.3 with KOH.

Cells were identified by morphology using fluorescent dyes Alexa Fluor-488 or Alexa Fluor-594 hydrazide added to the intracellular solution (10 μM; Invitrogen-ThermoFischer Scientific). Rod bipolar cells (RBCs) were characterized by their goblet-shaped somas localized in the external limit of the outer plexiform layer (OPL) and the extension of a single axon to the sublamina 5 (S5) of the inner plexiform layer (IPL), adjacent to the ganglion cell layer (GCL), where the axon ended in a series of varicosities. AII amacrine cells (ACs) were recognized by their diamond-shaped soma located at the INL/IPL border and by their bistratified dendritic trees formed by lobular appendages and arboreal dendrites at the distal and proximal parts of the IPL, respectively.[88] A17 ACs were distinguished by their large dome-shaped somas localized in the INL/IPL border and by their wide dendritic tree (~100 μm) which with present varicosities at regular intervals.[89–91] Retinal ganglion cells (RGCs) were identified by their large somas located in the GCL and no distinction between ON, ON-OFF, or OFF subtypes were made. Signals were recorded using a Multiclamp 700B amplifier (Molecular Devices), acquired at 10 kHz, and low-pass filtered at 2 kHz. Series (Rs) and input resistance (Rin) were continuously monitored throughout all the recordings and Rs was left uncompensated. Voltage values were not corrected for liquid junction potentials (~10 mV). Cells with changes in Rs >20% during the experiment were excluded from the analysis. Data were acquired and analyzed using a custom-made routine written in Igor Pro 6.37 (Wavemetrics, Portland, OR, USA).

All recordings started 2-3 min after break-in to allow cell dialysis and stabilization. Baseline recordings for spontaneous and evoked responses were performed for 5 min and drugs were bath applied for 10 min, except were indicated. Comparisons were performed between the last 2 min of the baseline and the last 2 min of the applied drug. Spontaneous excitatory postsynaptic currents (sEPSC) were recorded from AII and A17 ACs voltage-clamped at -60 mV in the continuous presence of SR95531 (10 μM), TPMPA (50 μM), strychnine (3 μM), APV (25 μM) and TTX (0.5 μM) to block $GABA_A$Rs, $GABA_C$Rs, GlyRs, NMDAR and NaV currents, respectively. Events were detected using the MINI analysis software (Synaptosoft). The threshold for event detection was set three times (~ -10 pA) above the root mean square noise level (~2-3 pA). Events were subsequently checked manually for accuracy. Excitatory postsynaptic currents (EPSC) were recorded from paired recordings between RBC and AII ACs and were evoked by depolarizing presynaptic RBC from -60 to -10 mV (100 ms; 20 s intervals). Such depolarization also triggers reciprocal GABAergic IPSC in RBCs.[28,92] For all evoked currents the amplitude was measured as the difference between the peak and the baseline, except for the vIPSC peak amplitude which was measured using the fitted baseline method (see Chavez et al.[28]). Inward Ca^{2+} currents were measured as the difference between the baseline and the last 20 ms of the inward current.

Two-photon calcium imaging/Image analysis

Experiments were obtained from RBCs and RGCs voltage-clamped at -60 mV in in presence of TTX (0.5 μM) and strychnine (3 μM). Red-fluorescent Alexa Fluor-594 (50 μM) and green-fluorescent calcium indicator Fluo-5F (300 μM) were included in the pipette solution to visualize cell morphology and changes of intracellular Ca^{2+} concentration, respectively. Imaging was performed in a two-photon laser-scanning microscope (Scientifica Hyperscope), equipped with a tunable wavelength Ti-Sapphire laser (Mai Tai DeepSee, Spectra-Physics). Fluorophores were excited using a wavelength of 810 nm, while emitted (reflected and transmitted) red and green photons were collected and separated by photomultiplier tubes. Calcium signal (ΔCa^{2+}) was observed at axon terminals of RBCs and RGCs dendrites and were elicited by a voltage depolarizing pulse (RBCs: 50 mV; RGCs: 70 mV) of 100 ms duration. Signals across terminals and dendrites were line scanned at 380 Hz. Plot profiles of the calcium signals were obtained with ImageJ, processed, and quantified in Igor 6.32 as increases in the green fluorescence from baseline normalized to the average red fluorescence (ΔG/R).

In vivo electroretinogram recordings

All experimental apparatus used for *in vivo* electroretinogram (ERG) recordings has been described in detail previously.[93] Briefly, animals were anesthetized with an intraperitoneal injection of ketamine hydrochloride (40 mg/kg) and xylazine (4 mg/kg) and maintained immobilized in a holder with the right eye pointing upward in a thermoregulated bed chamber at 32 ± 1°C. After local anesthesia with lidocaine (1%) and atropine sulfate (1%), an Ag/AgCl ring electrode was placed on the cornea and a subcutaneous platinum electrode on the skin was used as reference. Single-flash ERG responses were obtained under dark-adapted conditions prior to recording (no background illumination: 0 $\mu W/cm^2 sr$; 2 hrs.) and at different light flashes (1.230, 2.455, 4.786, 9.772, 19.498, 38.905, 77.625, 154.882, 316.228 and 630.957 photons/μm^2) with arbitrarily defined threshold intensity, expressed in the figures as log units (0.09, 0.39, 0.68, 0.99, 1.29, 1.59, 1.89, 2.19, 2.50 and 2.80, respectively). ERG responses were evoked by increasing the number of photons per flash (10 ms) with 10-s intervals between flashes at a fixed wavelength (λ=500 nm). All ERG responses were amplified, low- and high-pass filtered (1 Hz and 1000 Hz) with an AC/DC amplifier (A-M Systems, Model 3000, Carlsbourg, WA, USA), and digitalized with an analogue-digital interface (CB-68LP, National Instruments, Austin, TX, USA). Pharmacological agents were dissolved in phosphate buffer solution (PBS; pH= 7.4) and were administered by intravitreal injection of a 10 μL volume through a 30-gauge needle inserted at the pars plana region into the eye. In each animal, the right eye was initially used as a control and later injected intravitreally with either the vehicle (PBS/DMSO) or different pharmacological agents, including the CB1Rs agonist WIN 55,212-2 (WIN; 1 μM), the CB1 inverse agonist AM251 (4 μM), and the $GABA_A$ and $GABA_C$ receptors antagonist, SR-95531 (5 μM) and TPMPA (10 μM), respectively. All pharmacological agents were purchased from Sigma, Tocris and HelloBio. Final vitreal concentrations were estimated by assuming 0.15 ml vitreous volume[94] and full equilibration. Reagents were prepared in stock solutions (water or DMSO) and added to the PBS as needed. Total DMSO in the PBS solution was less than 0.01%.

Typically, rod-driven ERG response are composed of an electronegative component (a-wave) generated by the hyperpolarization of the photoreceptors and an electropositive component (b-wave) mainly generated by activity of ON bipolar cells.[95,96] ERG a- and b-wave amplitude were calculated by a polynomial fit, where the peak of response was compared to mean of 50 ms of baseline before of stimulus, using a custom-made analysis created in IGOR Pro Software (Wavemetrics, Oregon, USA). For all kinetics measurements (e.g. time to peak, half-width of decay ($T_{1/2D}$), and width), ERG responses were normalized to the mean of maximum response amplitude. The time to peak corresponds to the time from the onset of stimulus until the peak of response. The $T_{1/2D}$ represents the time from stimulus onset until half of the response decay, whereas the width indicates the time from half of rise until half of response decay. All ERG data are presented as mean ± SEM, and illustrated traces are averages of 5 flash responses.

QUANTIFICATION AND STATISTICAL ANALYSIS

All data are shown as mean ± S.E.M. The number of cells, animals and statistical significance for each analysis are specified in the figure legends. Statistical tests and exact p values are reported in Table S1. Normality of the data sets was tested using the Shapiro-Wilk test. For parametric data, two-group comparisons were performed using a paired t-test, and comparisons between more than two groups were performed with one-way ANOVA for repeated measures (ANOVA-RM), followed by a Tukey post-hoc test. For non-parametric data, comparisons between two groups were performed using the paired Wilcoxon rank test, and comparisons for more than two groups were performed using Friedman test, followed by the Wilcoxon-Nemenyi-McDonald-Thompson (WNMT) post-hoc test using Origin Pro 2018 (OriginLab, USA).